Supplementary Information for

Unassisted bipolar photoelectrochemical synthesis of H_2O_2

Haojie Chen,[1] Rui-Ting Gao,[1,2]* Lei Wang,[1]* Limin Wu [1,2]*

[1] College of Chemistry and Chemical Engineering, College of Energy Material and Chemistry, Inner Mongolia University, Hohhot 010021, China

[2] College of Smart Materials and Future Energy, Fudan University, Shanghai 200433, China

*To whom corresponding may be addressed.

E-mail: gao-ruiting@imu.edu.cn; wanglei@imu.edu.cn; lmw@fudan.edu.cn

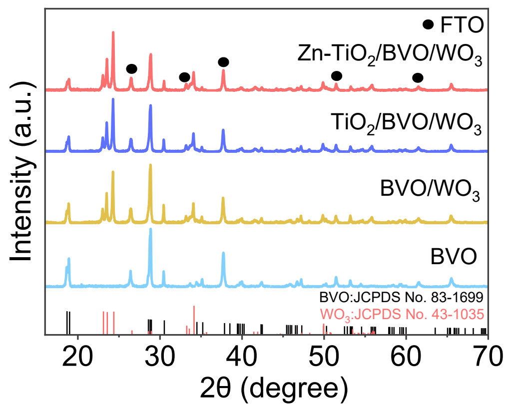

Supplementary Fig. 1 XRD patterns of BVO, BVO/WO_3, TiO_2/BVO/WO_3, and Zn-TiO_2/BVO/WO_3.

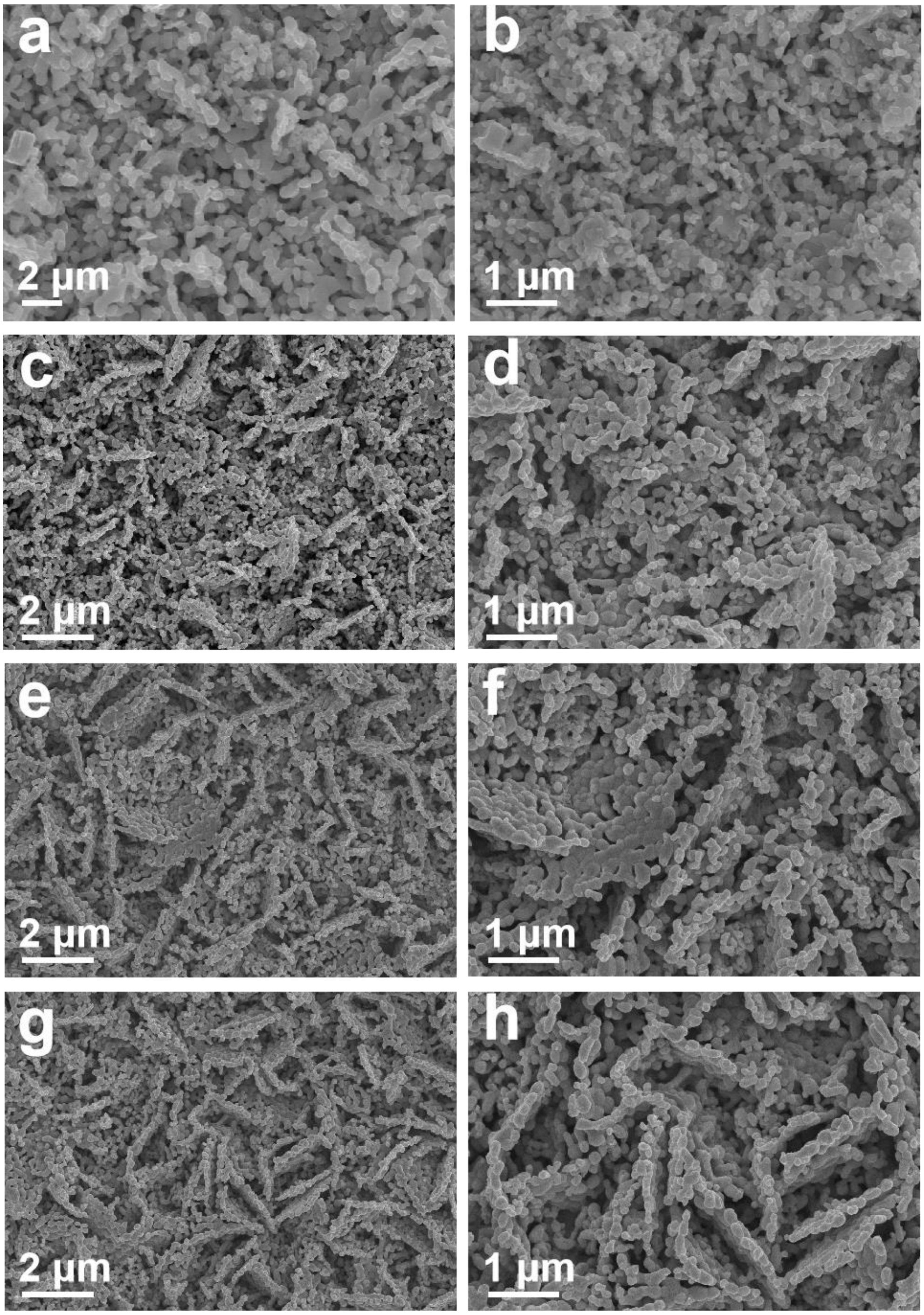

Supplementary Fig. 2 a-h SEM images of **a, b** BVO, **c, d** BVO/WO_3, **e, f** TiO_2/BVO/WO_3, and **g, h** Zn-TiO_2/BVO/WO_3.

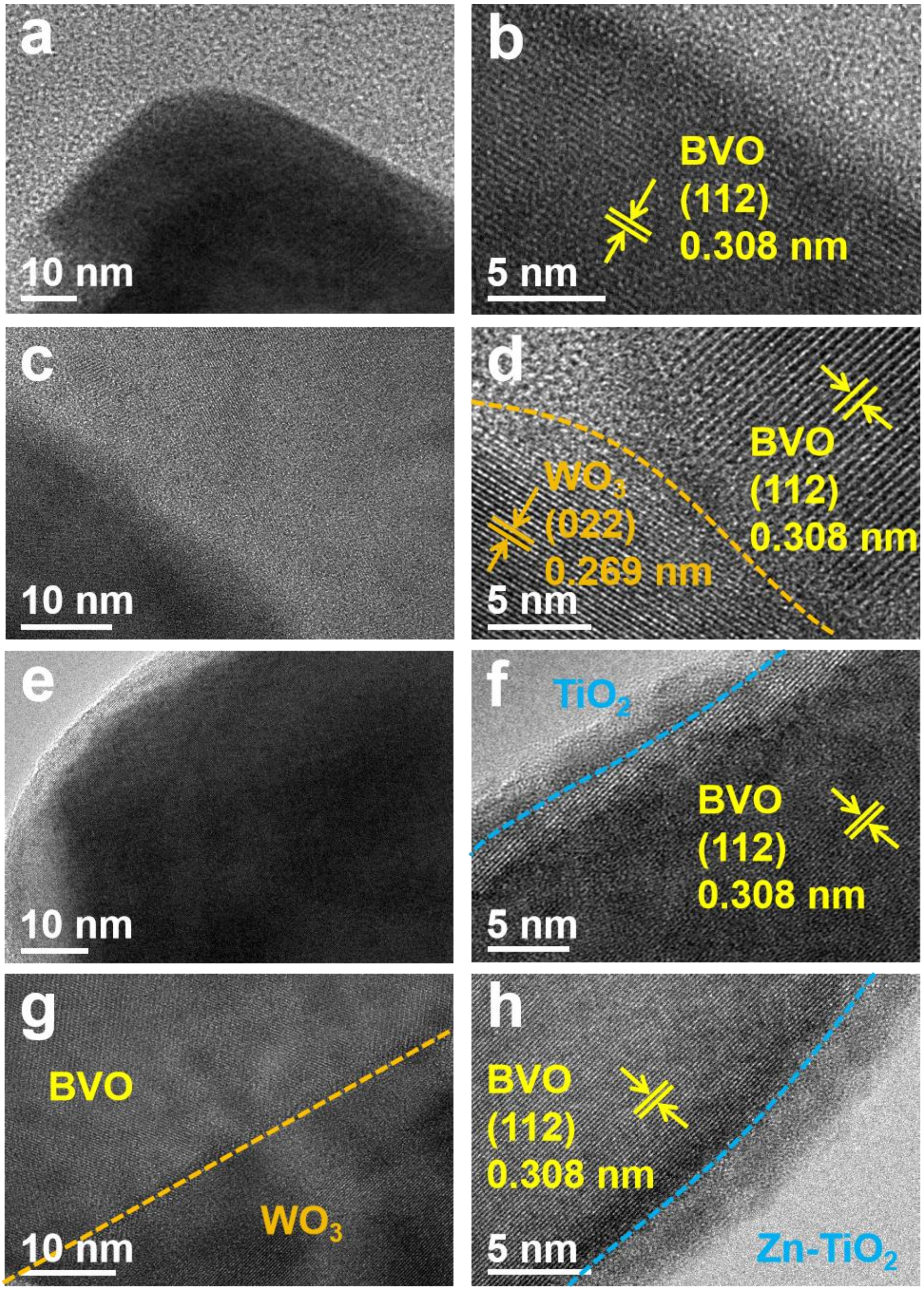

Supplementary Fig. 3 a-h TEM images of **a, b** BVO, **c, d** BVO/WO_3, **e, f** $TiO_2/BVO/WO_3$, and **g, h** $Zn\text{-}TiO_2/BVO/WO_3$.

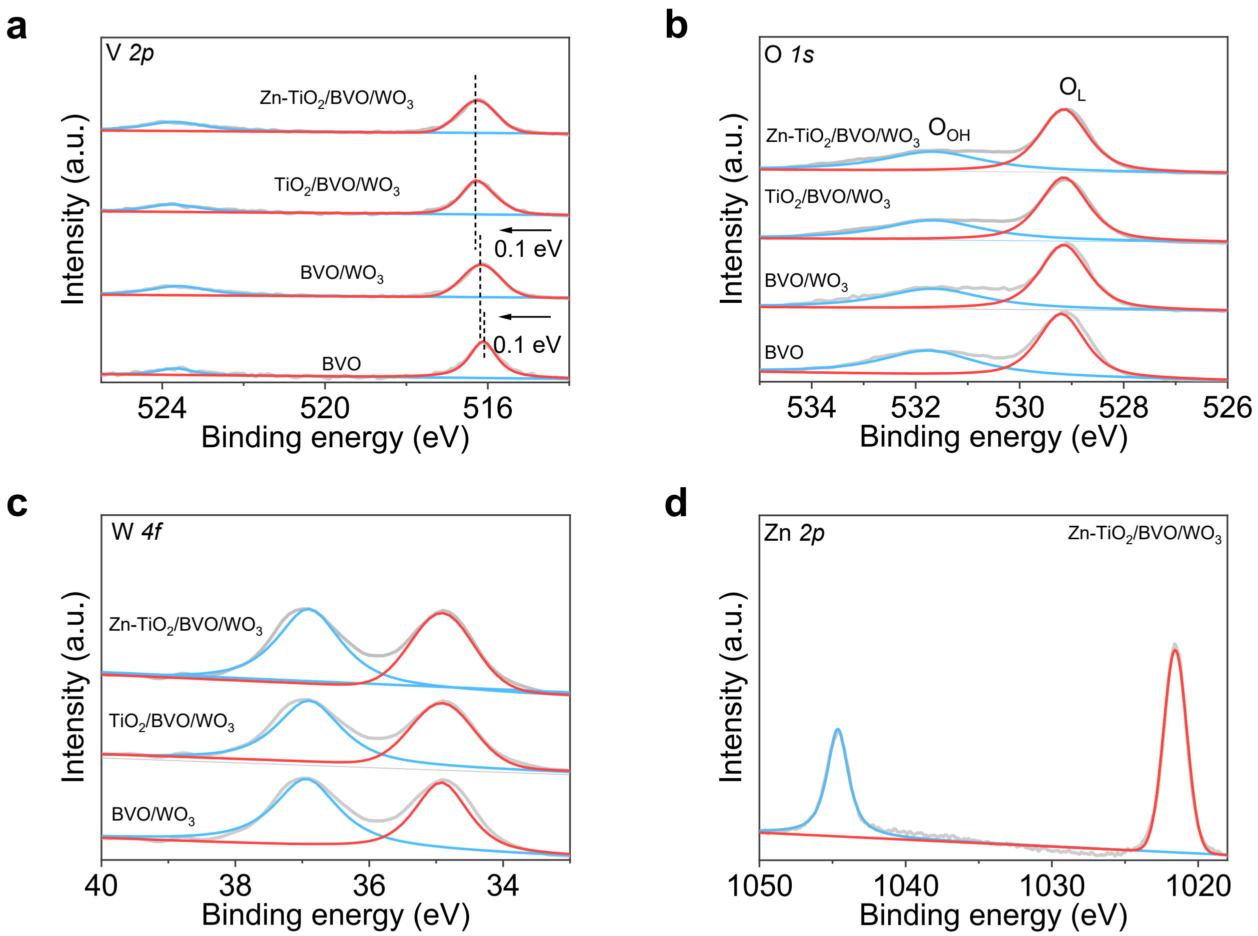

Supplementary Fig. 4 **a** V *2p*, **b** O *1s*, **c** W *4f*, and **d** Zn *2p* XPS spectra of BVO, BVO/WO_3, TiO_2/BVO/WO_3, and Zn-TiO_2/BVO/WO_3.

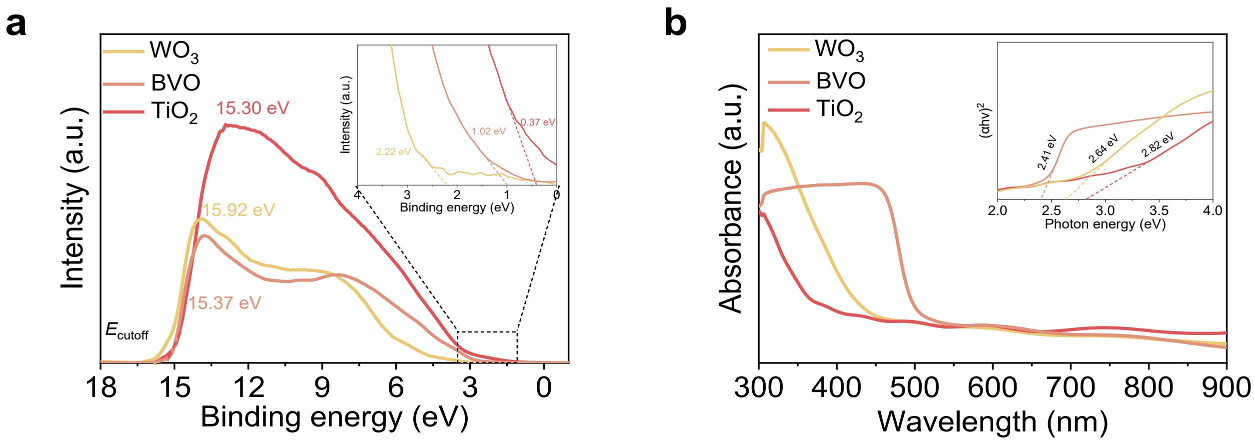

Supplementary Fig. 5 a UPS spectra of TiO_2, BVO, and WO_3. Inset shows the zoomed-in image area in the black dashed lines. **b** UV-vis spectra of TiO_2, BVO, and WO_3. Inset shows the optical band gaps.

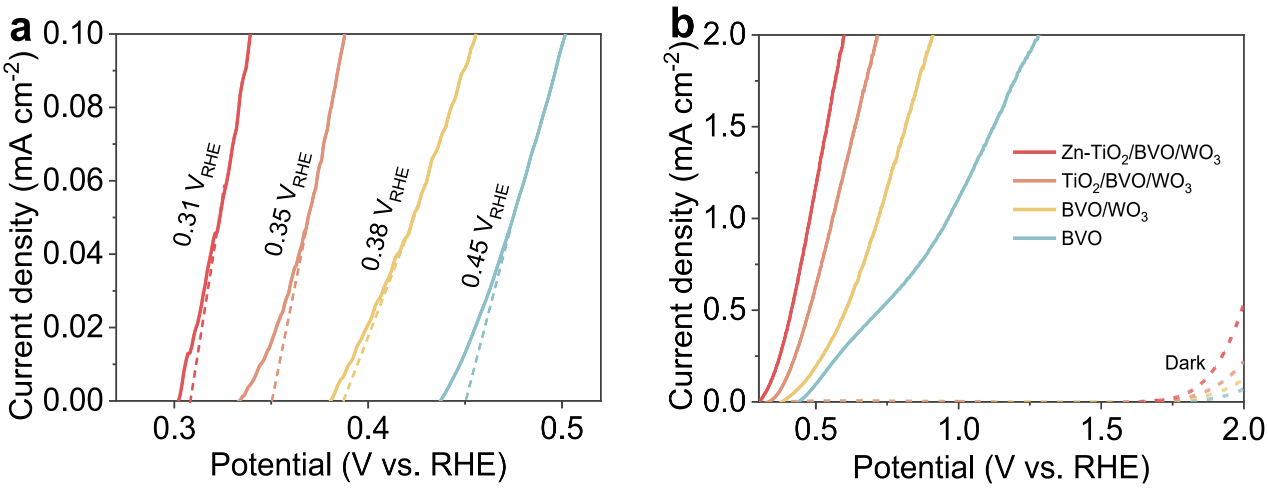

Supplementary Fig. 6 **a** Onset potentials (V_{on}) of BVO, BVO/WO_3, TiO_2/BVO/WO_3, and Zn-TiO_2/BVO/WO_3. **b** Potential shifts between dark and light current densities for the corresponding samples.

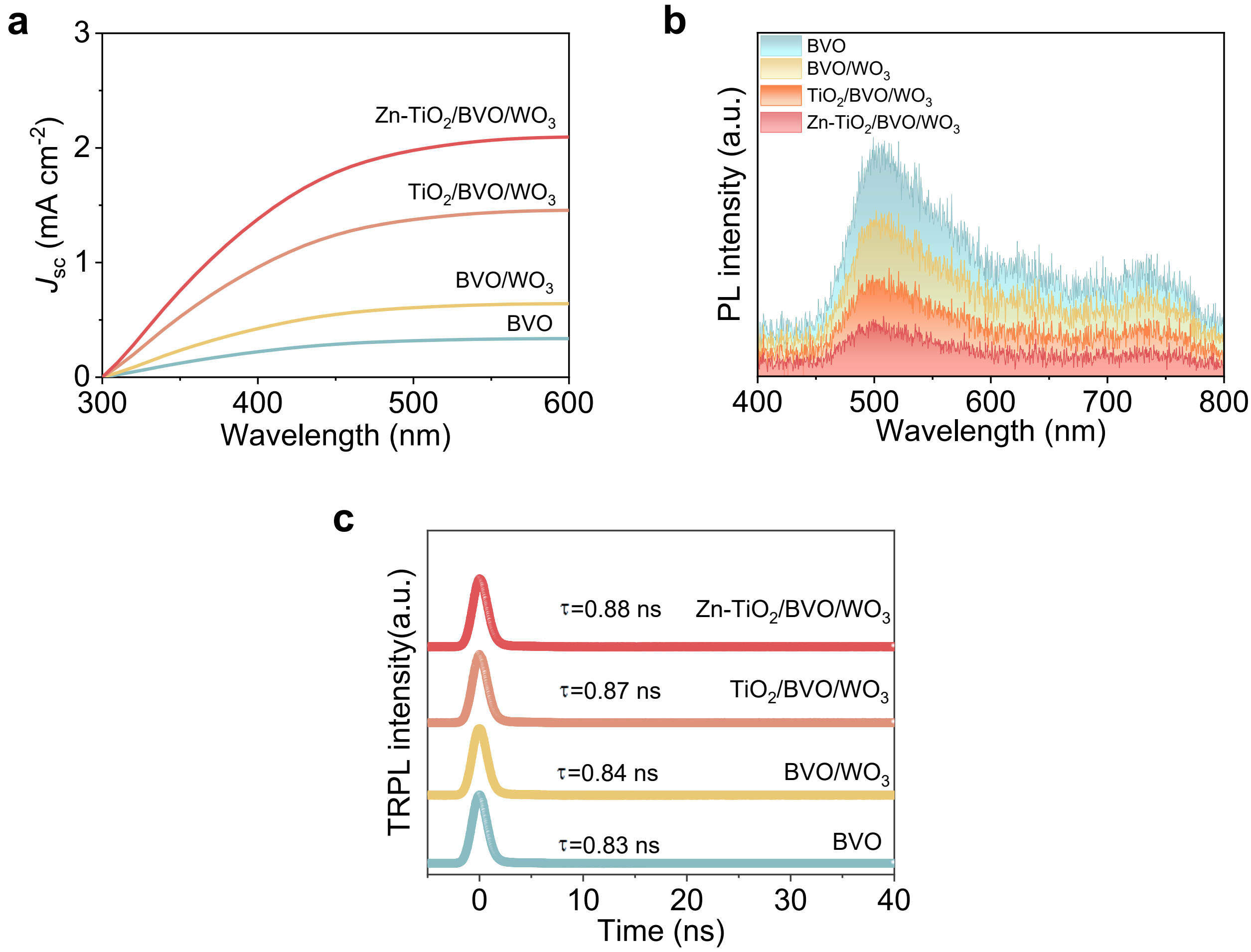

Supplementary Fig. 7 a Integrated photocurrent densities of BVO, BVO/WO_3, TiO_2/BVO/WO_3, and Zn-TiO_2/BVO/WO_3 measured at 0.6 V_{RHE}. **b** PL emission spectra and **c** TRPL decay spectra for the corresponding photoanodes.

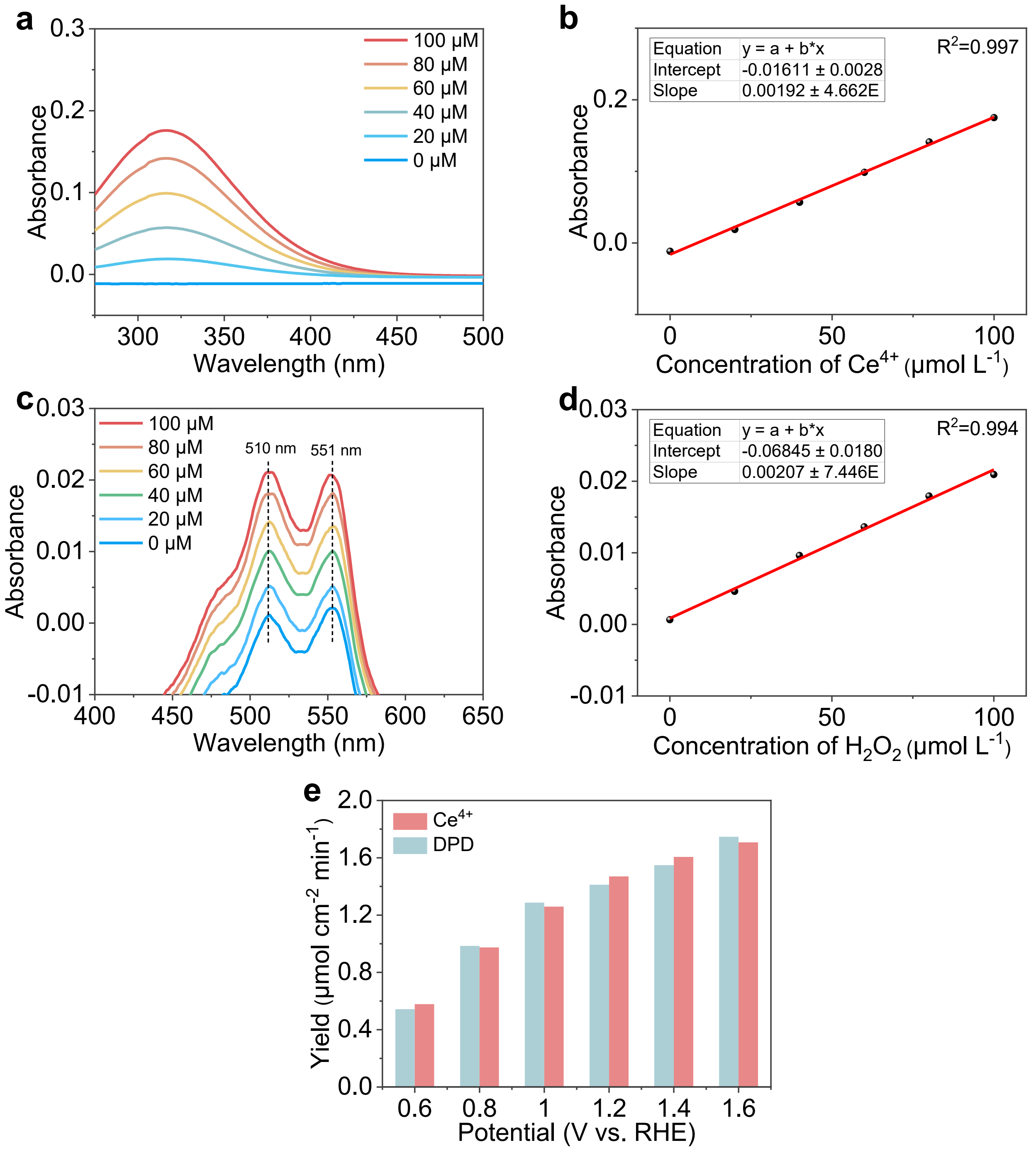

Supplementary Fig. 8 **a** UV-visible absorption spectra for various Ce^{4+} concentrations. **b** Fitting results of the absorbance vs. concentration. **c** The base of verification using standard 0 to 100 μM 30% H_2O_2. **d** Fitting results of the absorbance vs. concentration. **e** Yield rates of H_2O_2 at various applied potentials using the N, N-diethyl-p-phenylenediamine (DPD) colorimetric method and the Ce^{4+} method.[1,2]

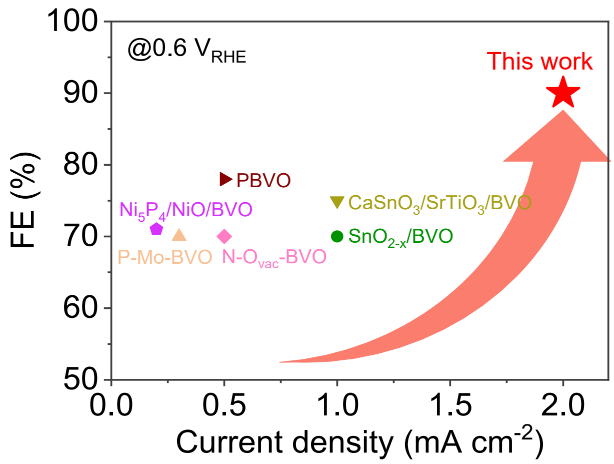

Supplementary Fig. 9 Comparison of H_2O_2 FEs and current densities with reported BVO photoanodes at 0.6 V_{RHE}.

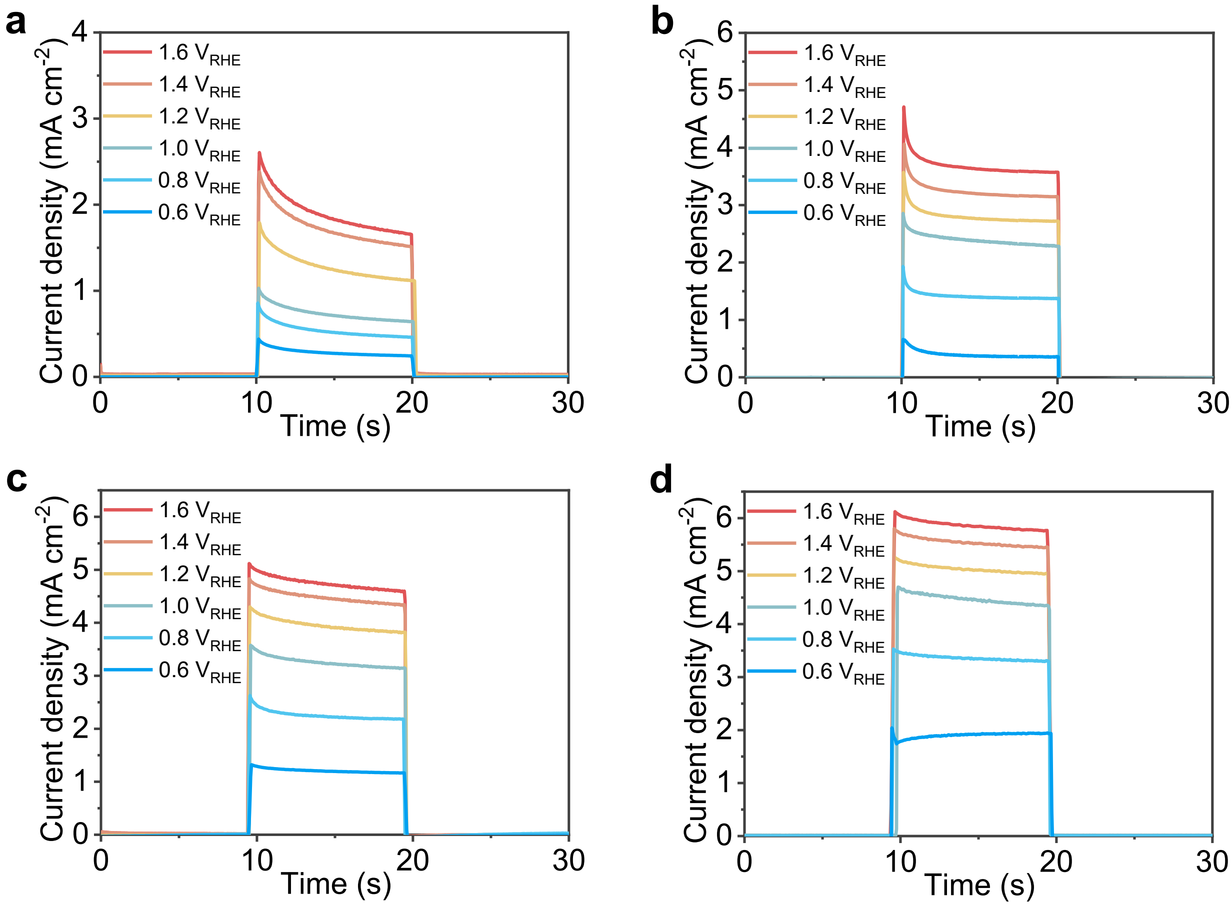

Supplementary Fig. 10 a-d Chopped-light photoresponses on **a** BVO, **b** BVO/WO_3, **c** TiO_2/BVO/WO_3, and **d** Zn-TiO_2/BVO/WO_3.

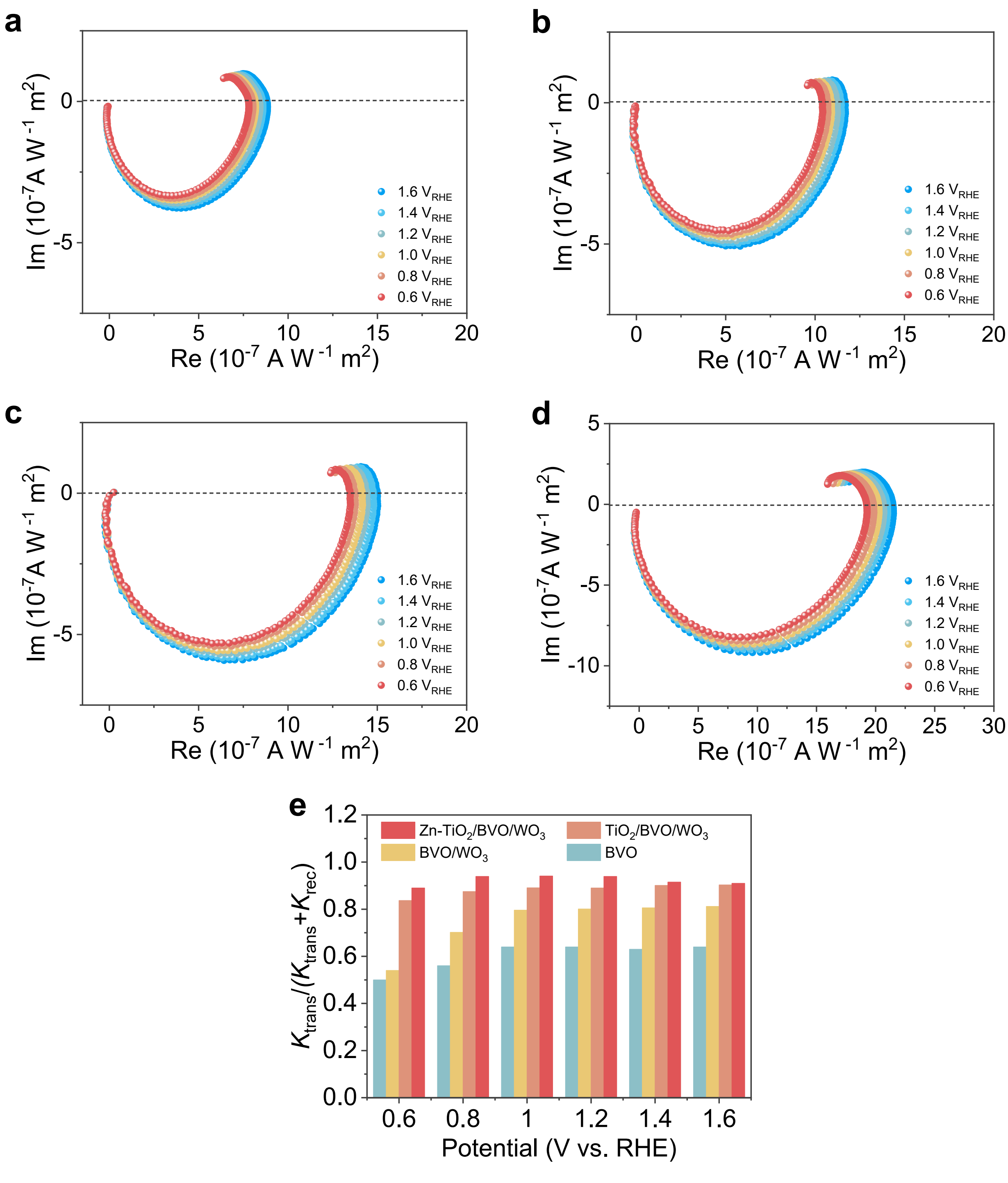

Supplementary Fig. 11 a-d IMPS responses of **a** BVO, **b** BVO/WO_3, **c** $TiO_2/BVO/WO_3$, and **d** Zn-$TiO_2/BVO/WO_3$ applied at various potentials. **e** Charge transfer efficiencies ($K_{trans}/(K_{trans}+K_{rec})$) derived from IMPS for the corresponding samples.

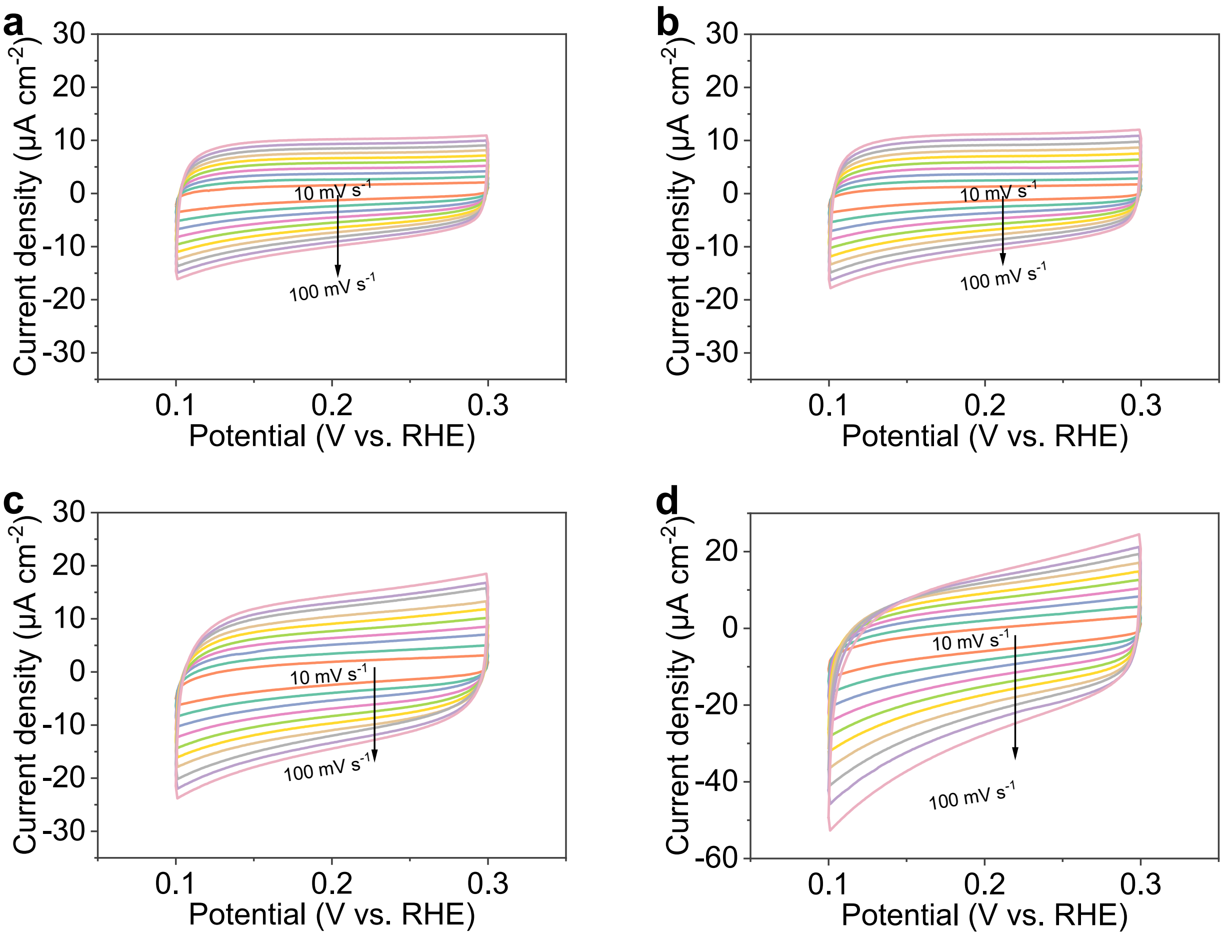

Supplementary Fig. 12 a-d Cyclic voltammetry curves of **a** BVO, **b** BVO/WO_3, **c** $TiO_2/BVO/WO_3$, and **d** Zn-$TiO_2/BVO/WO_3$.

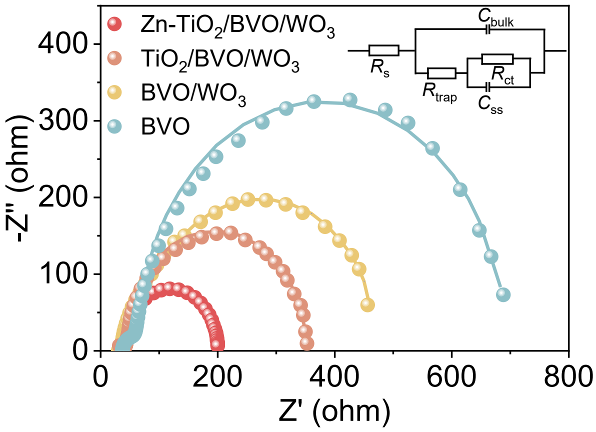

Supplementary Fig. 13 EIS measurements for BVO, BVO/WO_3, $TiO_2/BVO/WO_3$, and Zn-$TiO_2/BVO/WO_3$. Inset shows the corresponding circuit model.

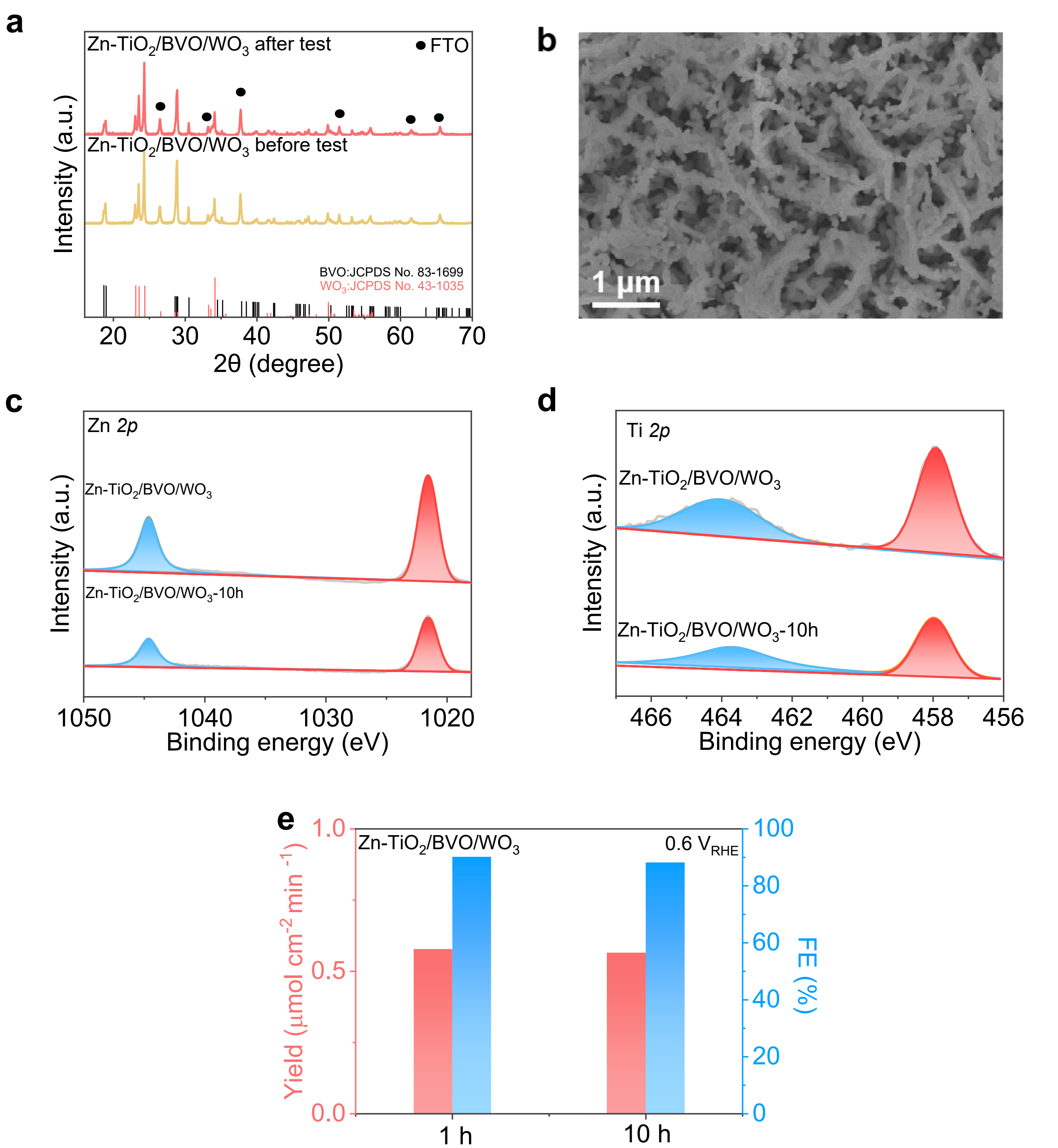

Supplementary Fig. 14 a XRD patterns for Zn-TiO_2/BVO/WO_3 before and after stability. **b** SEM image for Zn-TiO_2/BVO/WO_3 after stability. **c** Zn *2p* and **d** Ti *2p* XPS spectra of Zn-TiO_2/BVO/WO_3 before and after stability. **e** FEs and yields of H_2O_2 for Zn-TiO_2/BVO/WO_3 before and after stability.

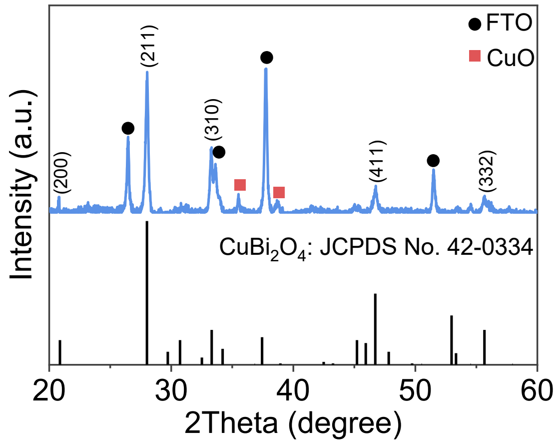

Supplementary Fig. 15 XRD pattern of Ru:CuO/Nb-CBO.

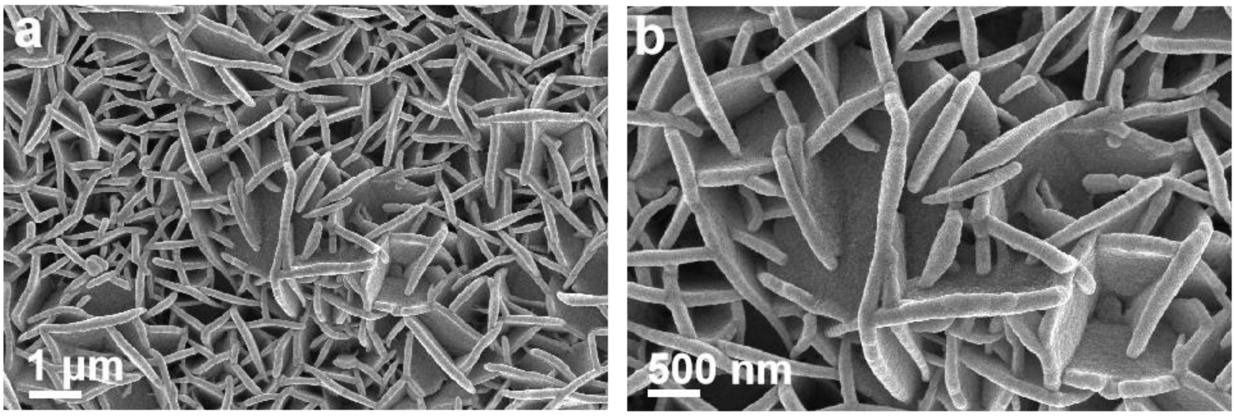

Supplementary Fig. 16 a and **b** SEM images of Ru:CuO/Nb-CBO.

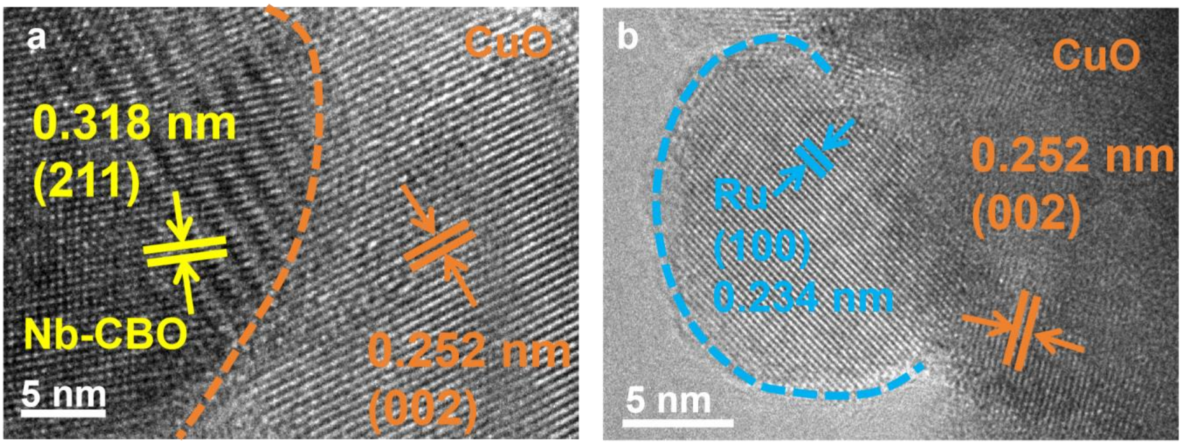

Supplementary Fig. 17 a and **b** TEM images of Ru:CuO/Nb-CBO.

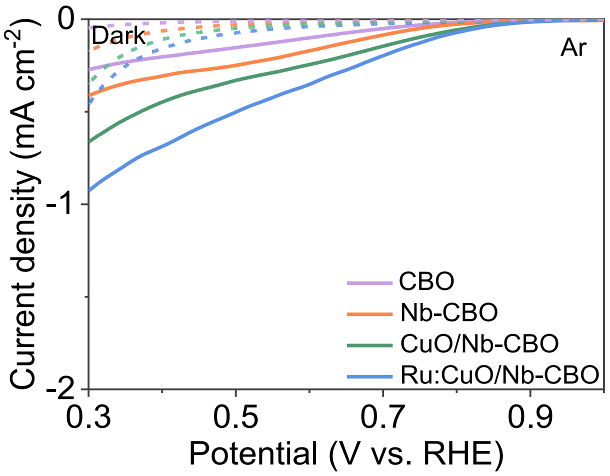

Supplementary Fig. 18 LSV curves of CBO, Nb-CBO, CuO/Nb-CBO, and Ru:CuO/Nb-CBO in Ar-saturated electrolytes.

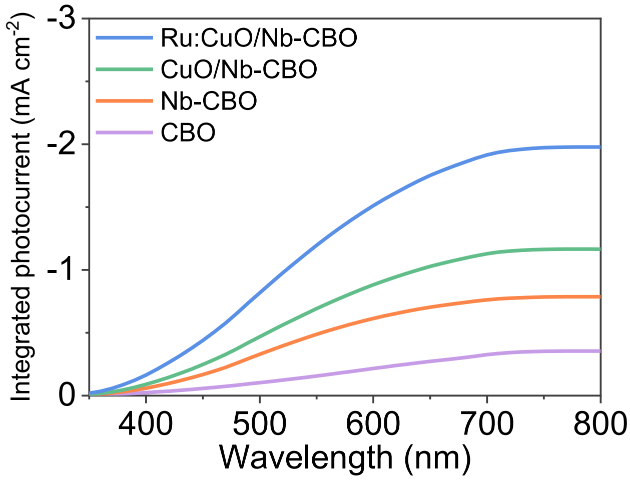

Supplementary Fig. 19 Integrated photocurrent densities of CBO, Nb-CBO, CuO/Nb-CBO, and Ru:CuO/Nb-CBO measured at 0.6 V_{RHE}.

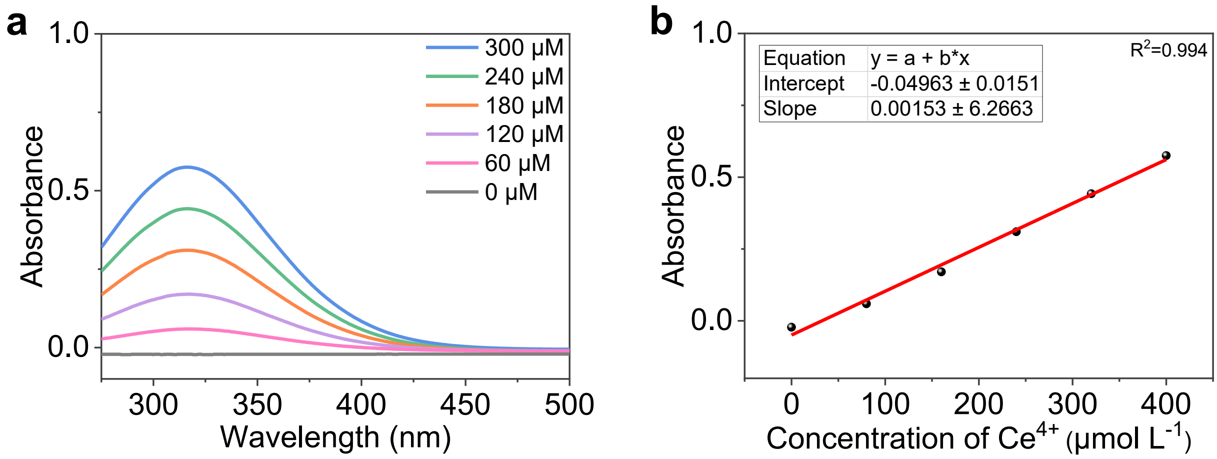

Supplementary Fig. 20 a UV-visible absorption spectra for various Ce^{4+} concentrations. **b** Fitting results of the absorbance vs. concentration.

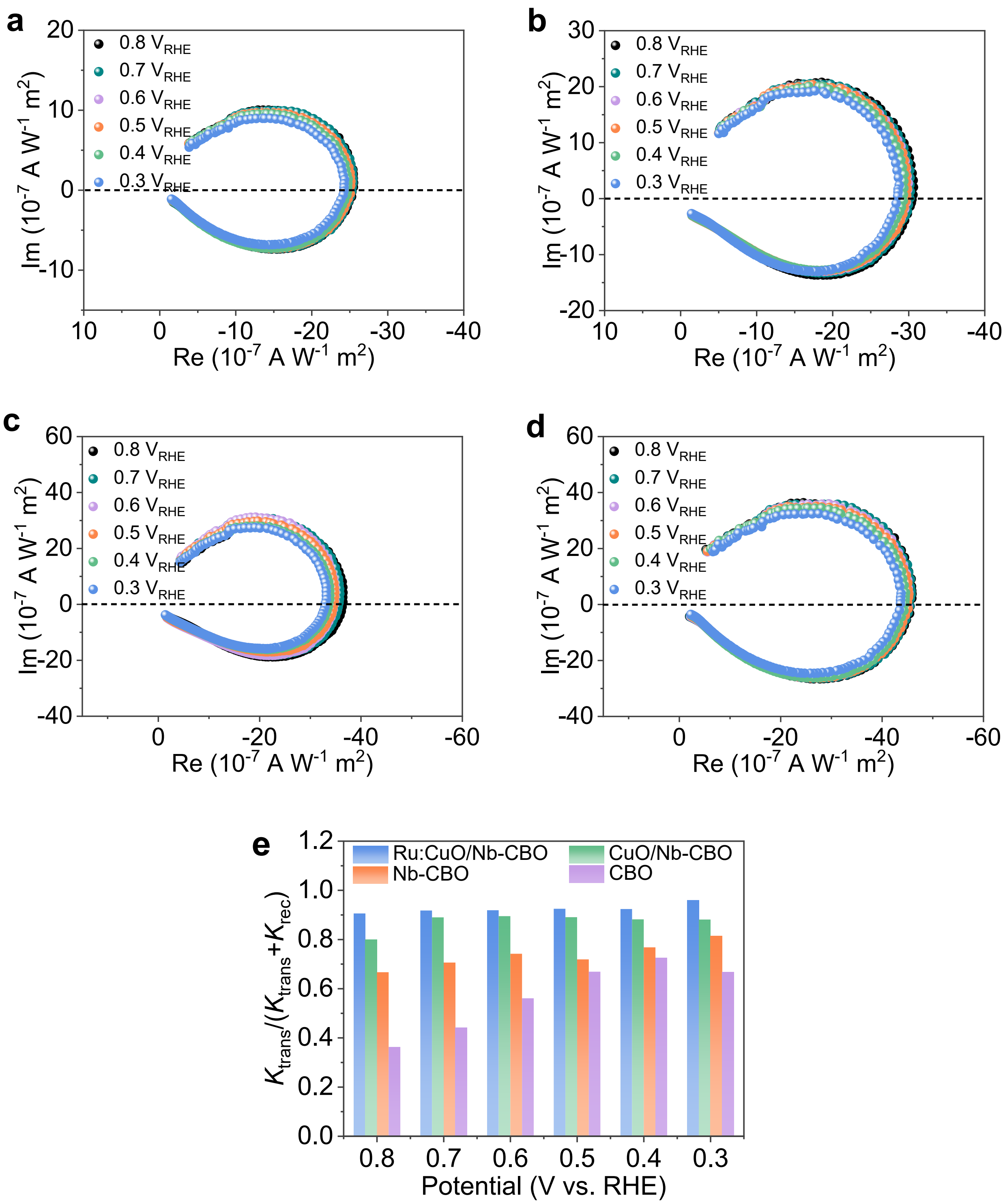

Supplementary Fig. 21 a-d IMPS responses of **a** CBO, **b** Nb-CBO, **c** CuO/Nb-CBO, and **d** Ru:CuO/Nb-CBO applied at various potentials. **e** Charge transfer efficiencies ($K_{trans}/(K_{trans}+K_{rec})$) derived from IMPS data for the corresponding samples.

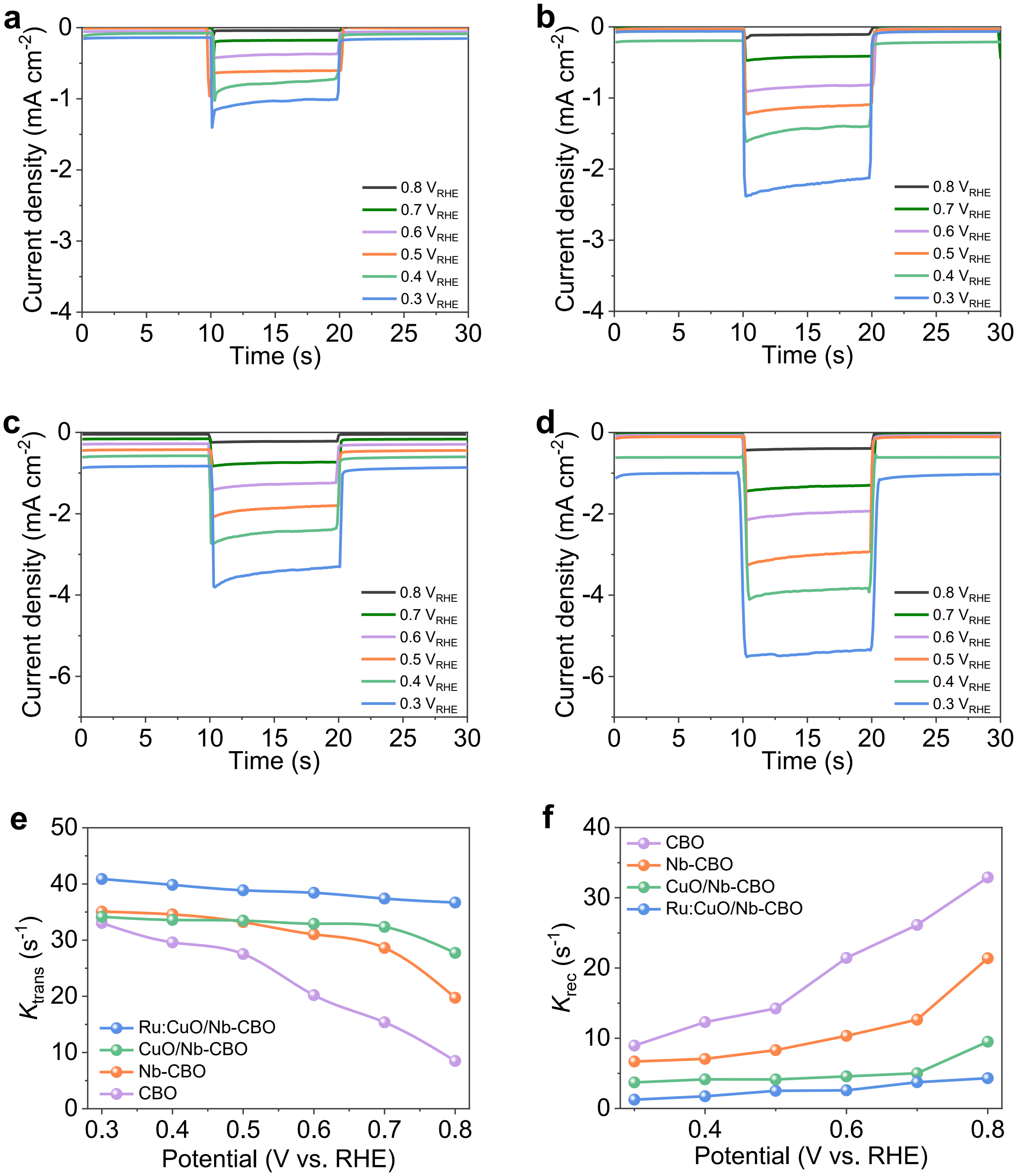

Supplementary Fig. 22 a-d Chopped-light photoresponses on **a** CBO, **b** Nb-CBO, **c** CuO/Nb-CBO, and **d** Ru:CuO/Nb-CBO. **e** Charge transfer (K_{trans}) and **f** charge recombination (K_{rec}) rate constants from IMPS spectra.

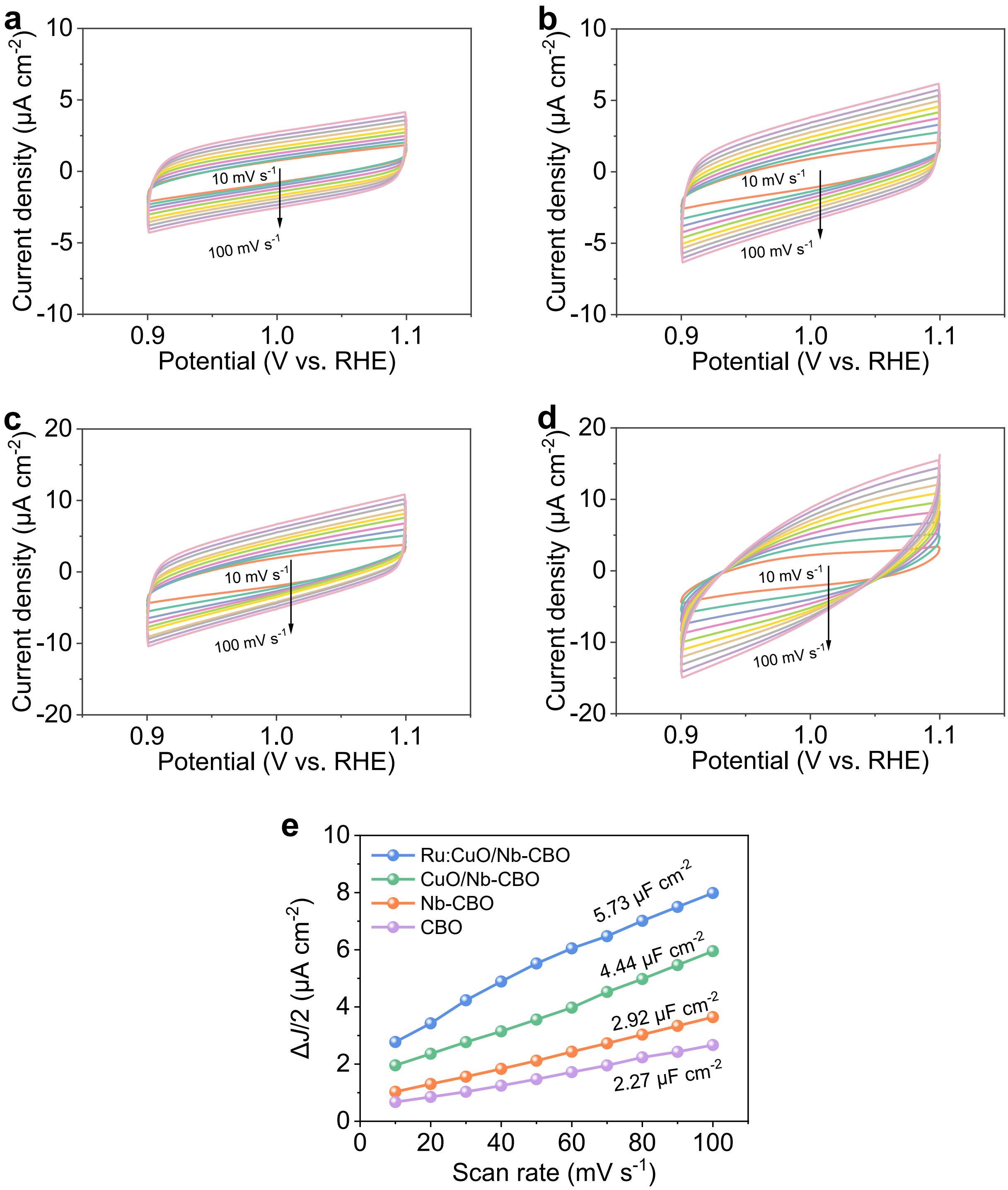

Supplementary Fig. 23 a-d Cyclic voltammetry curves of **a** CBO, **b** Nb-CBO, **c** CuO/Nb-CBO, and **d** Ru:CuO/Nb-CBO. **e** C_{dl} plots for the corresponding samples.

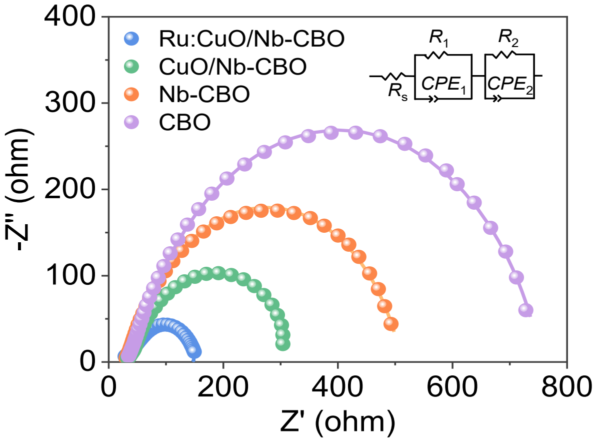

Supplementary Fig. 24 EIS measurements for CBO, Nb-CBO, CuO/Nb-CBO, and Ru:CuO/Nb-CBO.

Inset shows the corresponding circuit model.

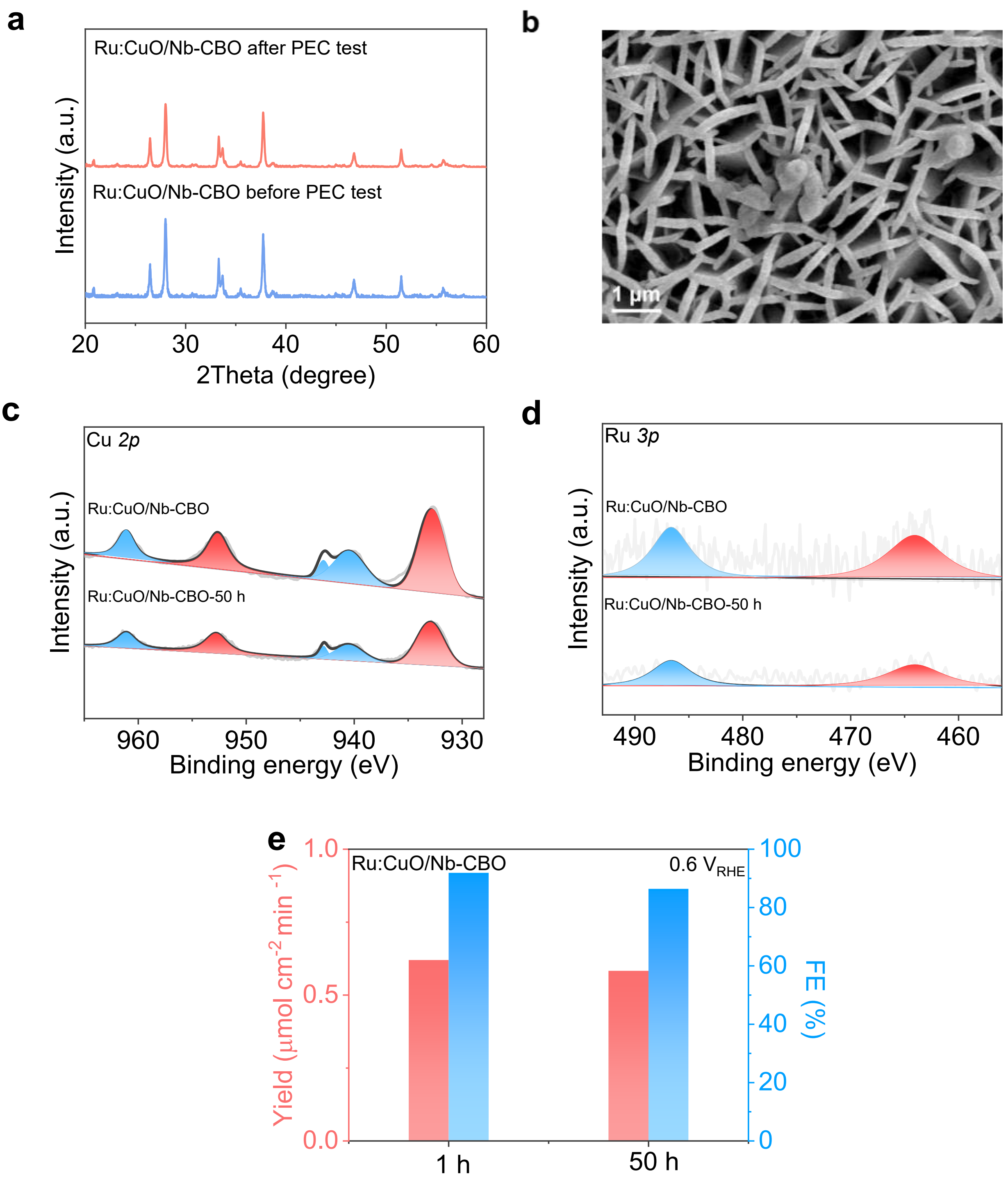

Supplementary Fig. 25 a XRD patterns for Ru:CuO/Nb-CBO before and after stability. **b** SEM image for Ru:CuO/Nb-CBO after stability. **c** Cu *2p* and **d** Ru *3p* XPS spectra of Ru:CuO/Nb-CBO before and after stability. **e** FEs and yields of H_2O_2 of Ru:CuO/Nb-CBO before and after stability.

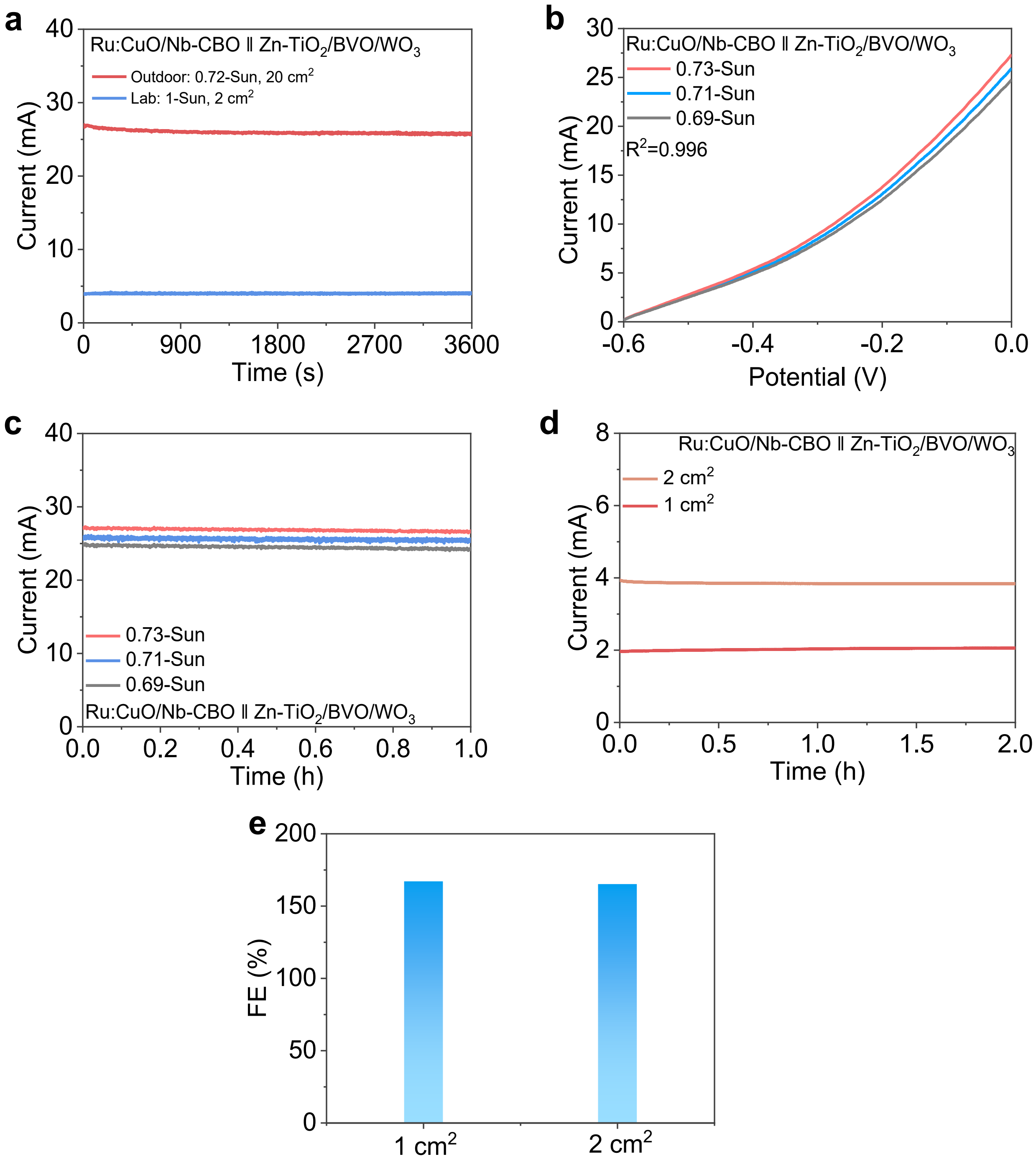

Supplementary Fig. 26 a Comparison of *I-t* curves of Ru:CuO/Nb-CBO ‖ Zn-TiO_2/BVO/WO_3 in the lab and outdoor conditions. **b** Three independent repeated LSV curves measured under different sunlight intensities. The surface areas of photoelectrodes are 20 cm^2. **c** Three independent repeated i-t curves measured under different sunlight intensities. **d** Chronoamperometry of unbiased Ru:CuO/Nb-CBO ‖ Zn-TiO_2/BVO/WO_3 (no membrane). The surface areas of photoelectrodes were 1 cm^2 and 2

cm^2. **e** H_2O_2 FEs for cells (no membrane).

Supplementary Discussion: we have performed stability tests for small-scale cells under membrane-free conditions. For 1 cm^2 and 2 cm^2 cells (no membrane), the system maintains stable photocurrent and H_2O_2 production for over 2 h, with total FEs of 167.12% and 162.23%, respectively (Supplementary Fig. 26d and e).

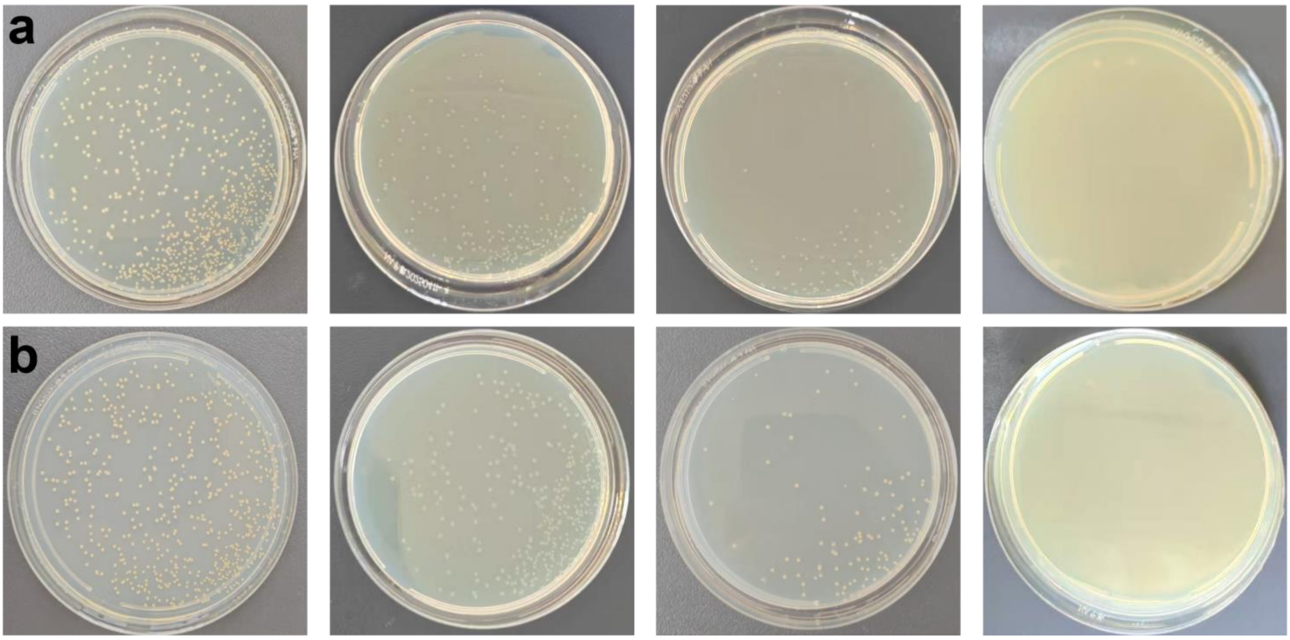

Supplementary Fig. 27 a, b Colony number of **a** *E. coli* and **b** *S. aureus* at 0, 20, 40, and 60 min, respectively.

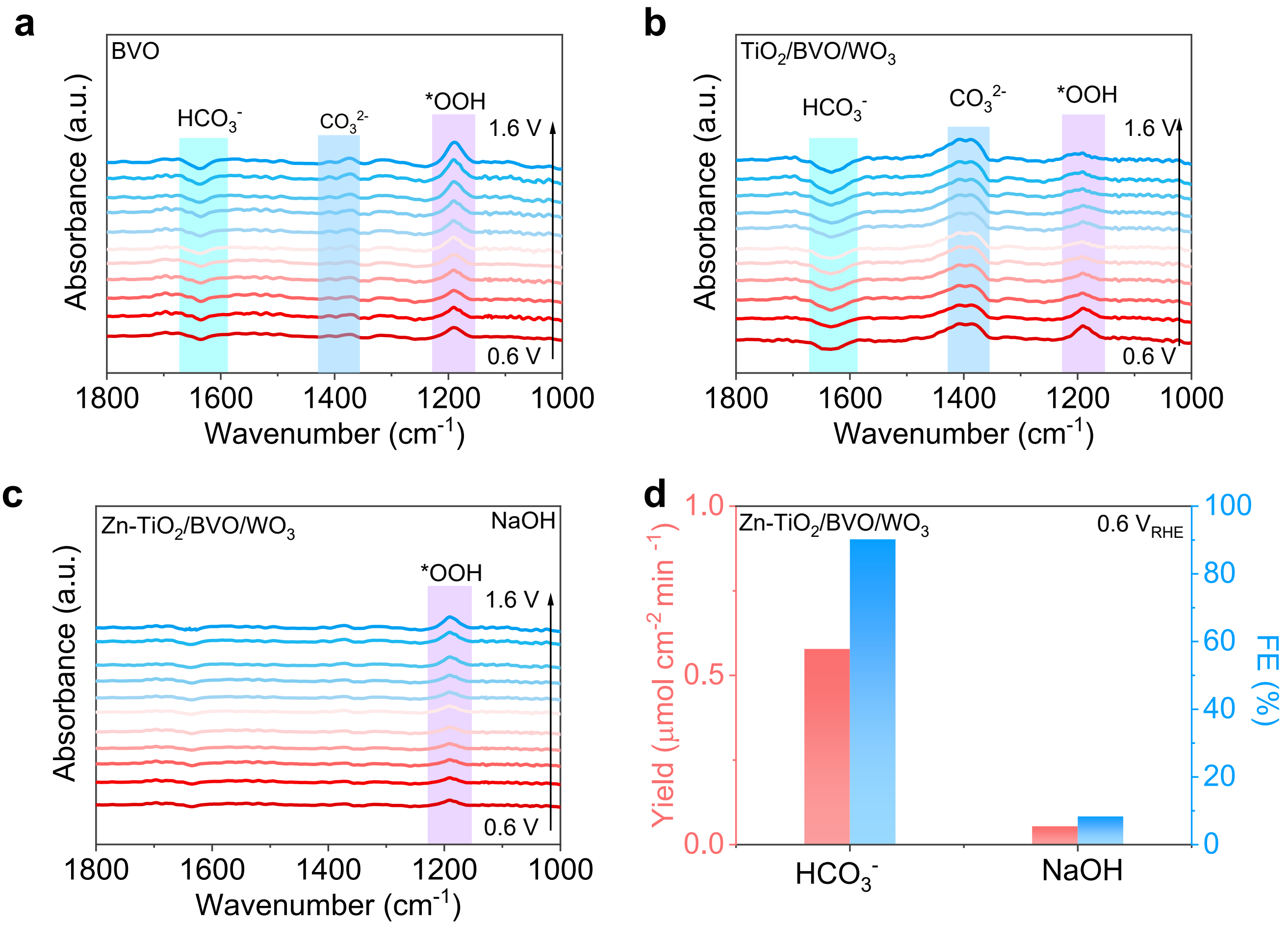

Supplementary Fig. 28 a, b *In situ* ATR-SEIRAS spectra recorded on **a** BVO and **b** $TiO_2/BVO/WO_3$. **c** *In situ* ATR-SEIRAS spectra of adsorbed intermediates recorded on Zn-$TiO_2/BVO/WO_3$ in bicarbonate-free electrolyte. **d** FEs and yields of H_2O_2 for Zn-$TiO_2/BVO/WO_3$ at various electrolytes.

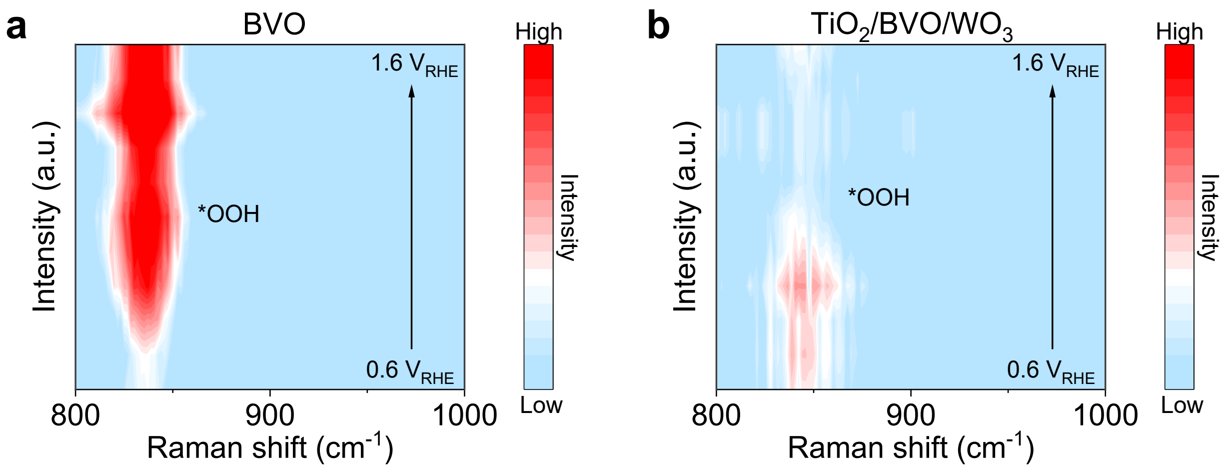

Supplementary Fig. 29 a, b *In situ* Raman spectra of **a** BVO and **b** TiO_2/BVO/WO_3.

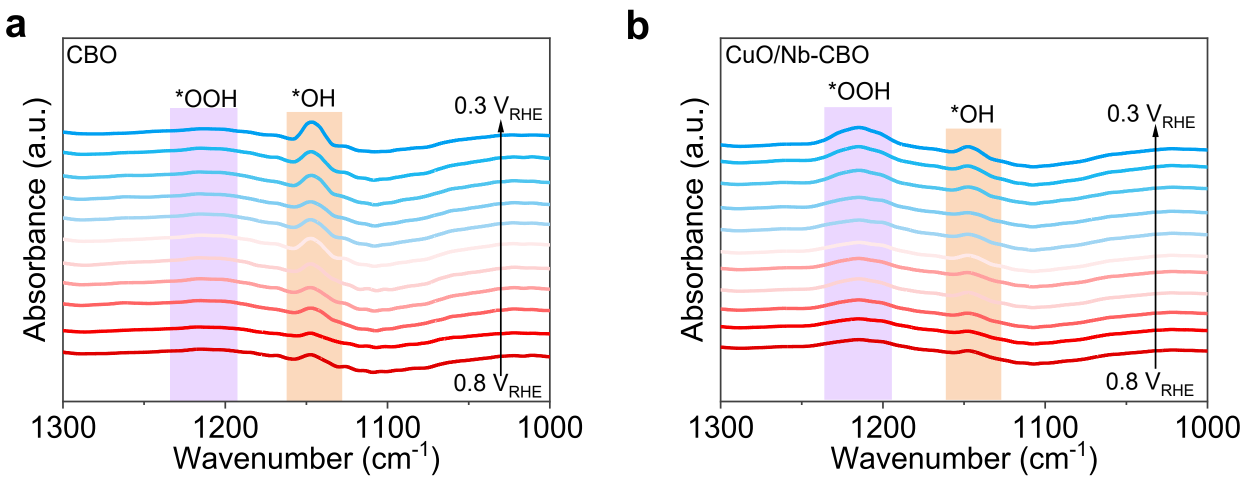

Supplementary Fig. 30 a, b *In situ* ATR-SEIRAS spectra recorded on **a** CBO and **b** CuO/Nb-CBO.

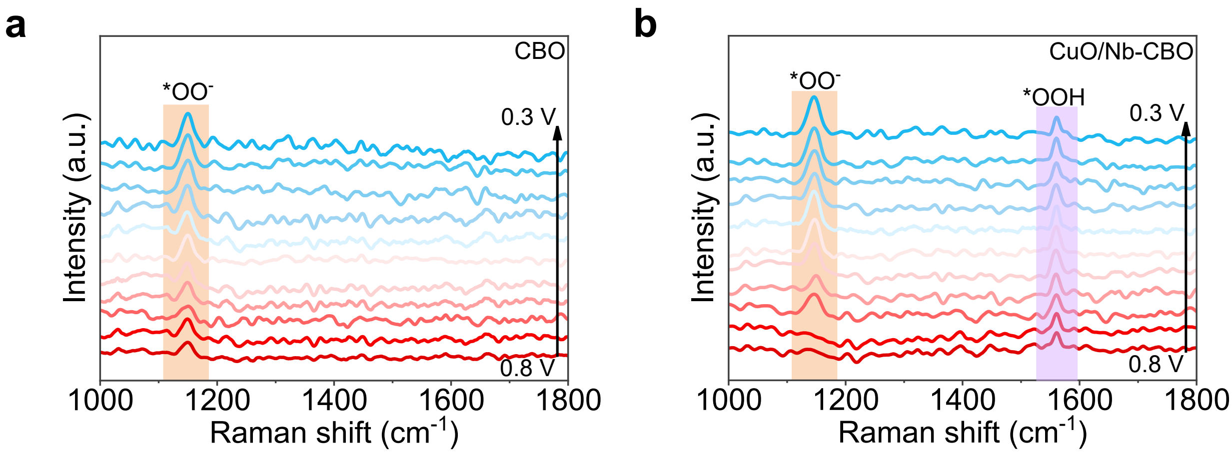

Supplementary Fig. 31 a,b *In situ* Raman spectra of **a** CBO and **b** CuO/Nb-CBO.

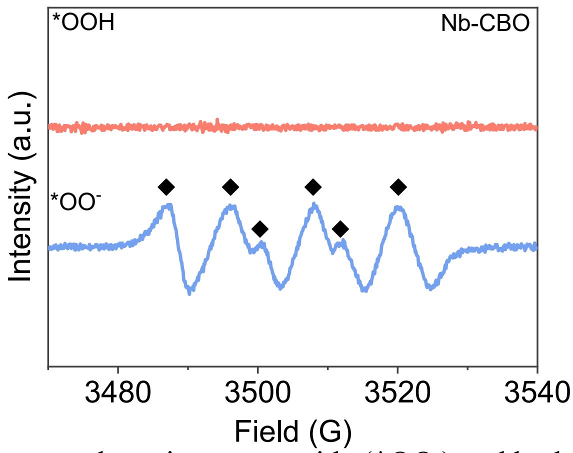

Supplementary Fig. 32 EPR spectra detecting superoxide (*OO$^-$) and hydroperoxyl (*OOH) radicals on Nb-CBO.

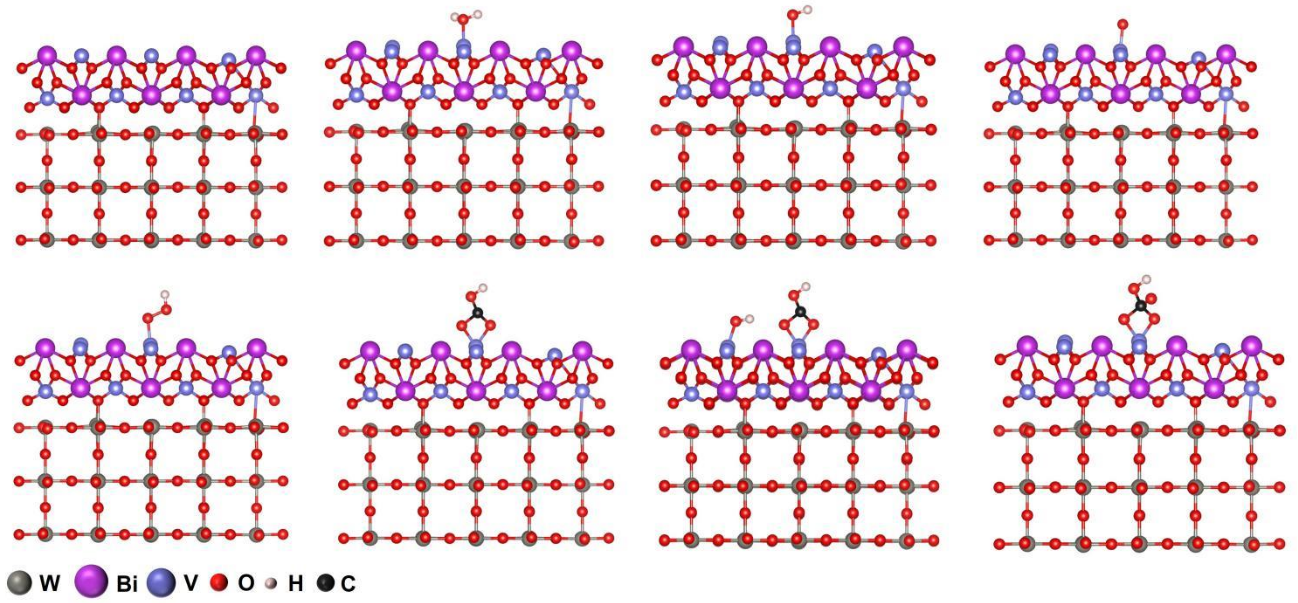

Supplementary Fig. 33 Optimized atomic configurations of each step for the WOR over BVO/WO_3 established based on the catalytic surface modeling of BVO/WO_3.

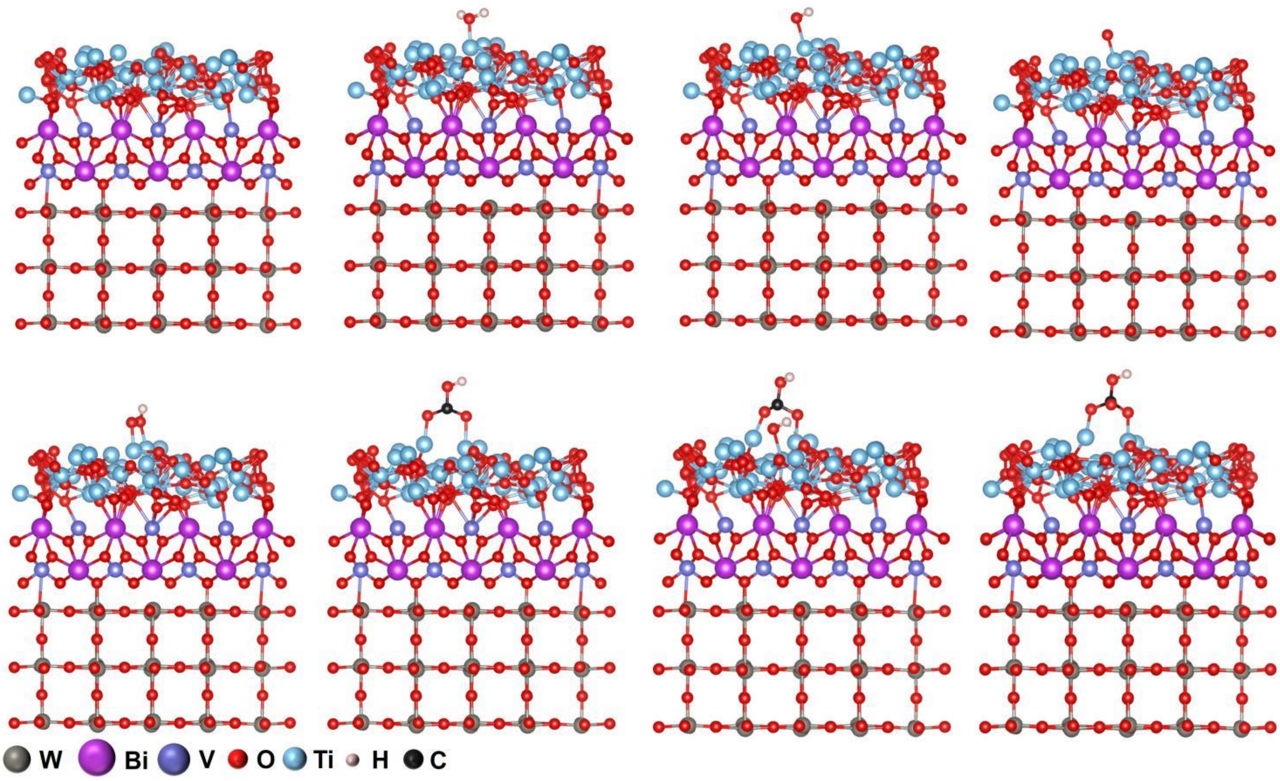

Supplementary Fig. 34 Optimized atomic configurations of each step for the WOR over TiO_2/BVO/WO_3 established based on the catalytic surface modeling of TiO_2/BVO/WO_3.

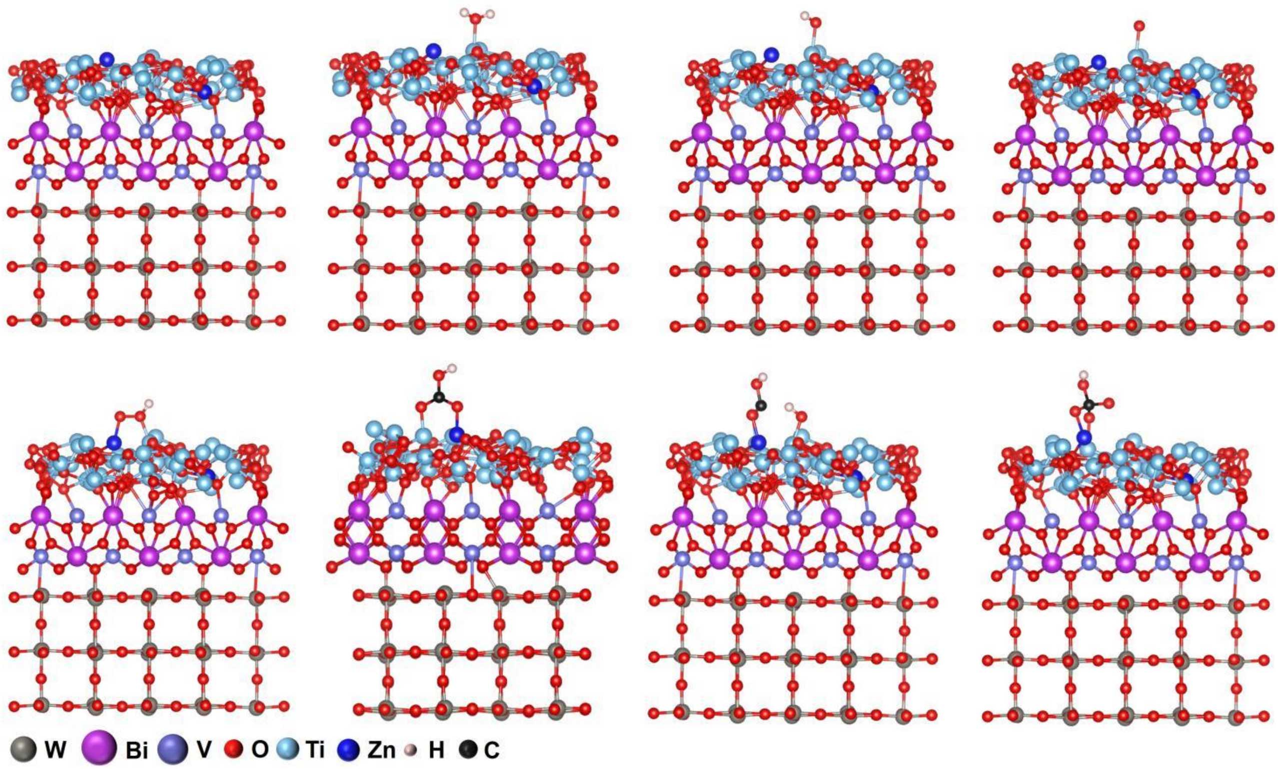

Supplementary Fig. 35 Optimized atomic configurations of each step for the WOR over Zn-TiO_2/BVO/WO_3 established based on the catalytic surface modeling of Zn-TiO_2/BVO/WO_3.

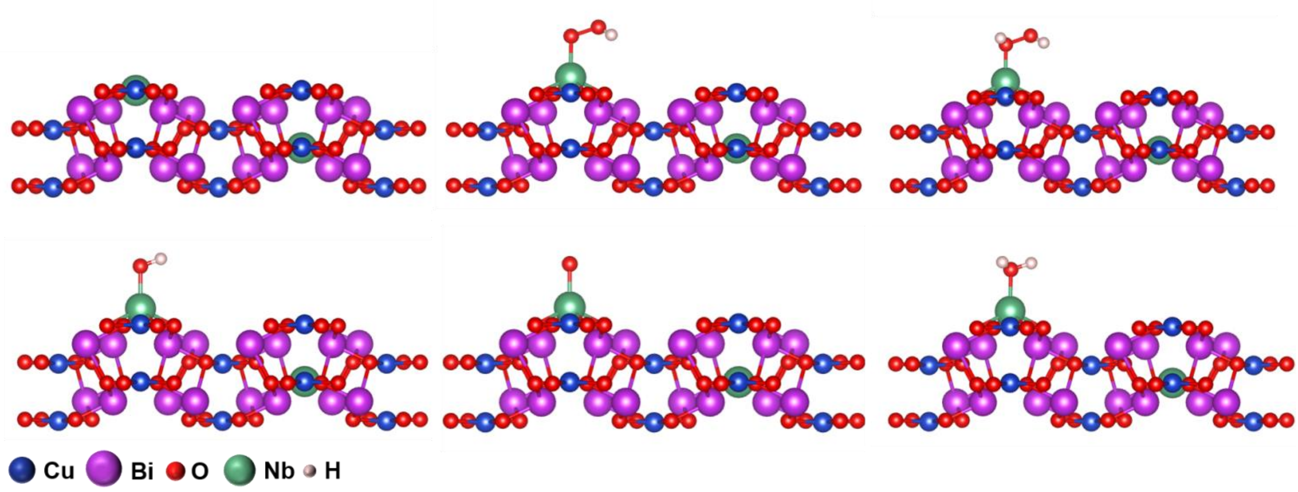

Supplementary Fig. 36 Optimized atomic configurations of each step for the ORR over Nb-CBO established based on the catalytic surface modeling of Nb-CBO.

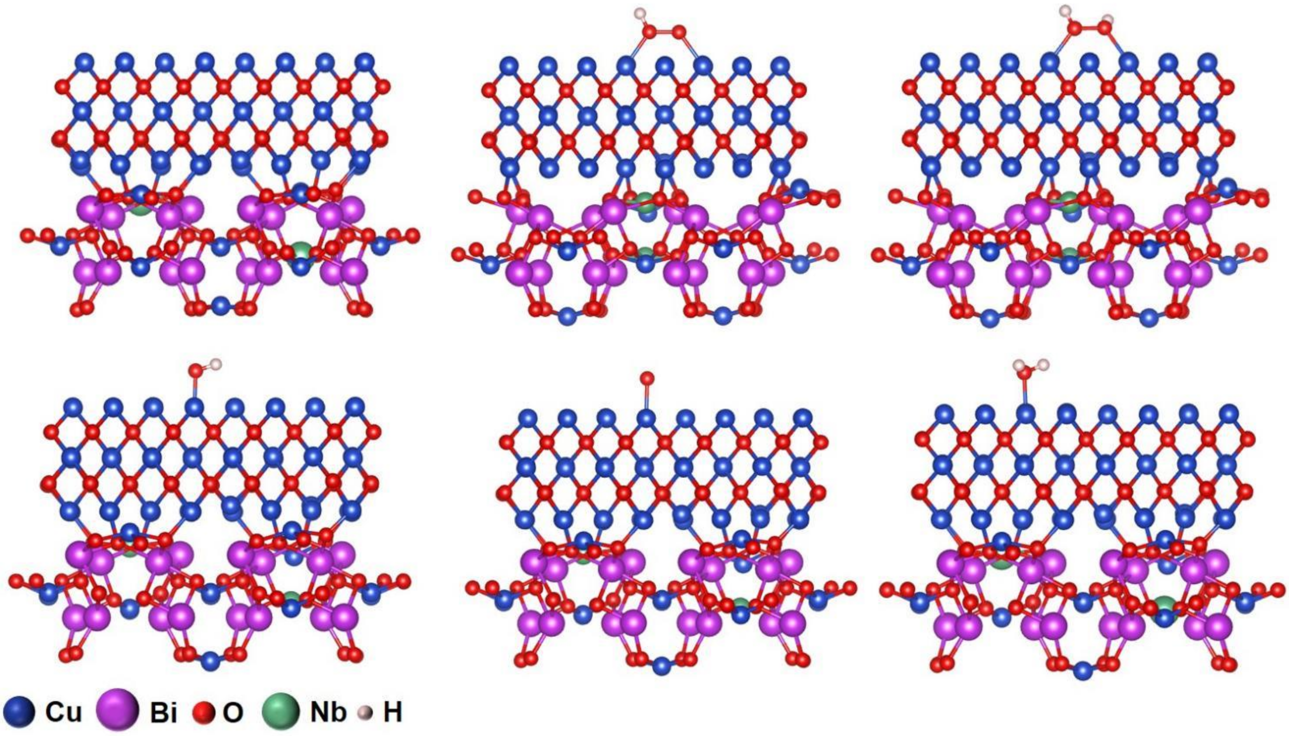

Supplementary Fig. 37 Optimized atomic configurations of each step for the ORR over CuO/Nb-CBO established based on the catalytic surface modeling of CuO/Nb-CBO.

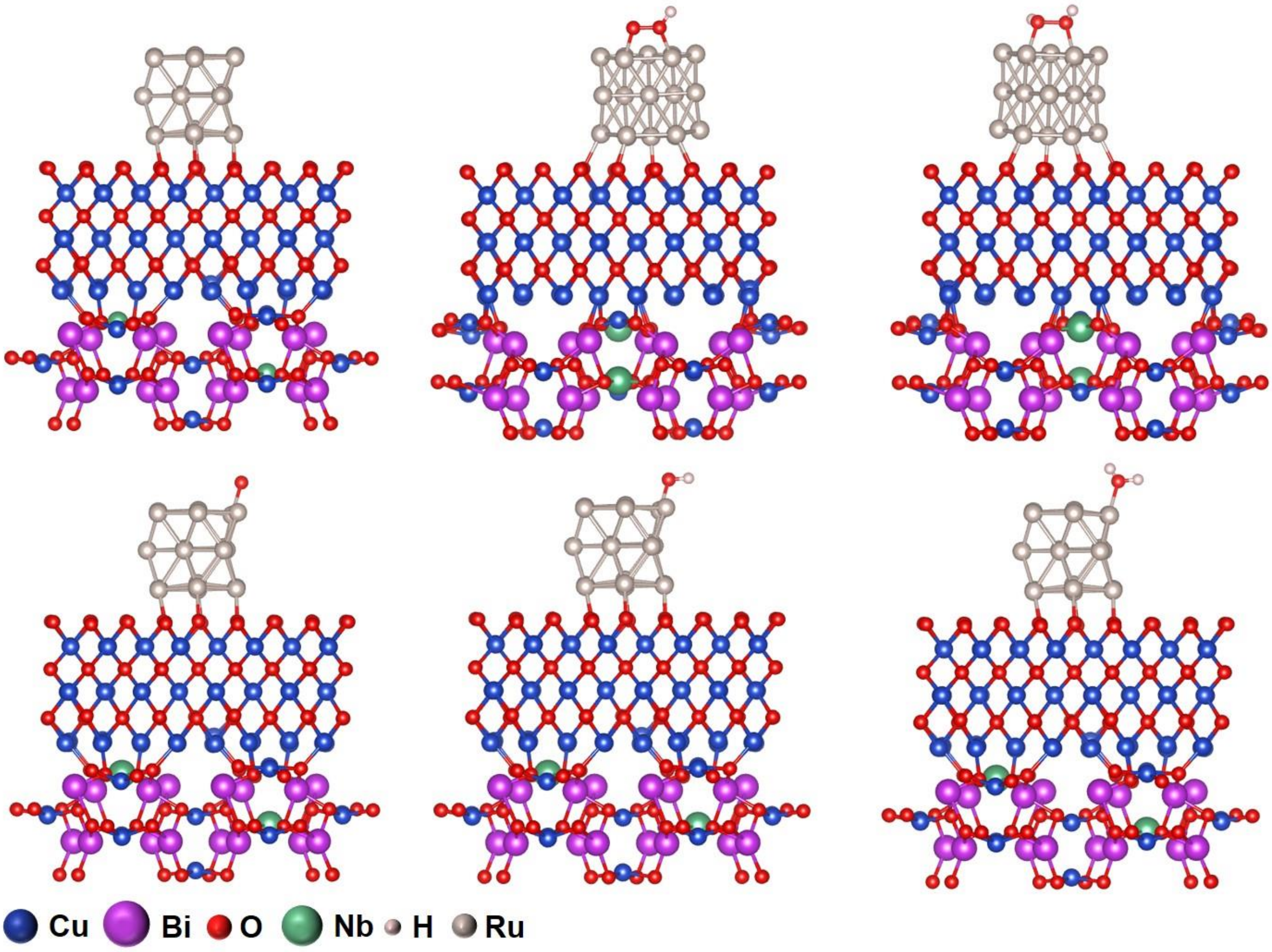

Supplementary Fig. 38 Optimized atomic configurations of each step for the ORR over Ru:CuO/Nb-CBO established based on the catalytic surface modeling of Ru:CuO/Nb-CBO.

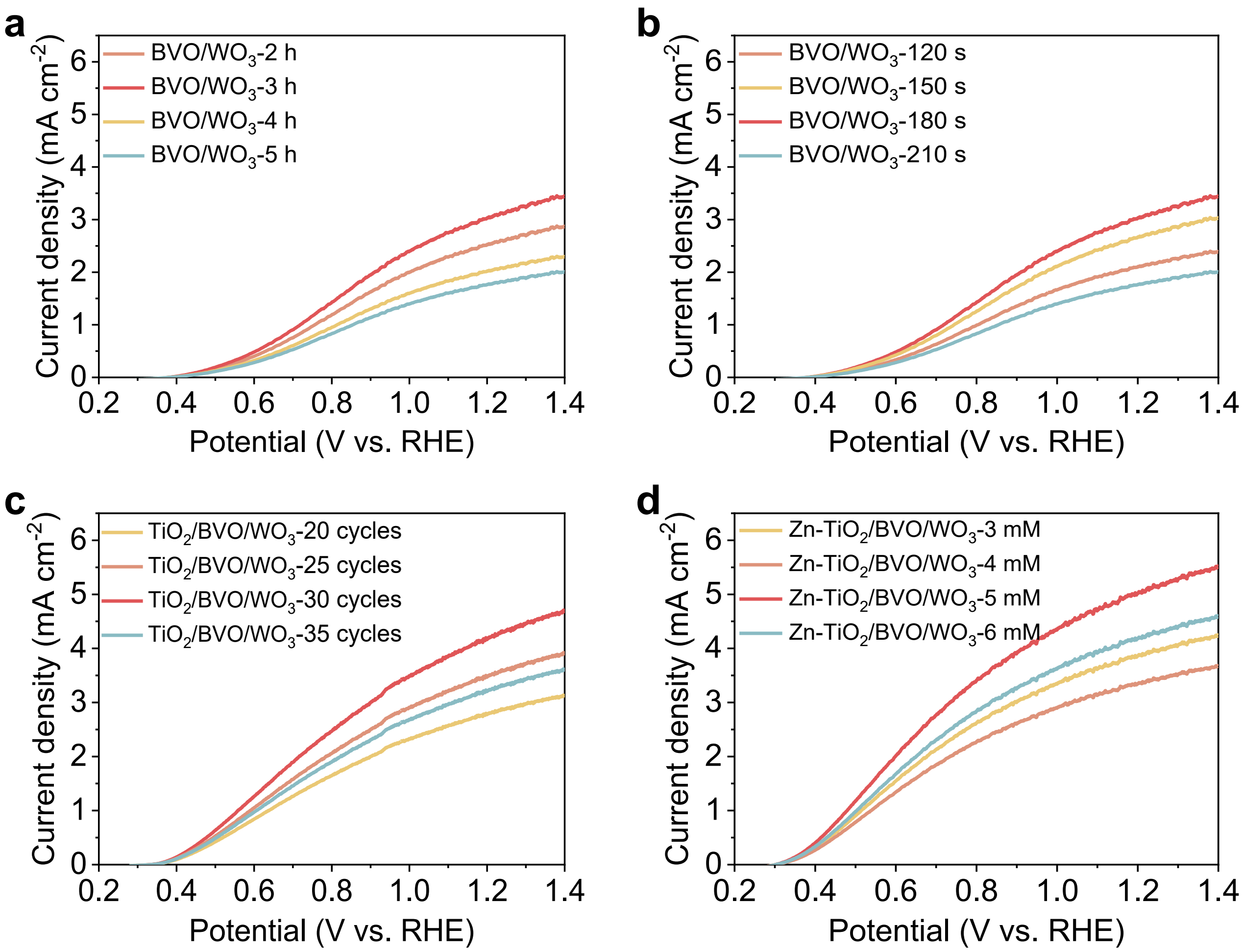

Supplementary Fig. 39 a LSV curves of BVO/WO_3 with various hydrothermal times for WO_3. **b** LSV curves of BVO/WO_3 with various deposition times for BVO. **c** LSV curves of $TiO_2/BVO/WO_3$ with various deposition cycle for TiO_2. **d** LSV curves of Zn-$TiO_2/BVO/WO_3$ with various $Zn(NO_3)_2$ concentrations.

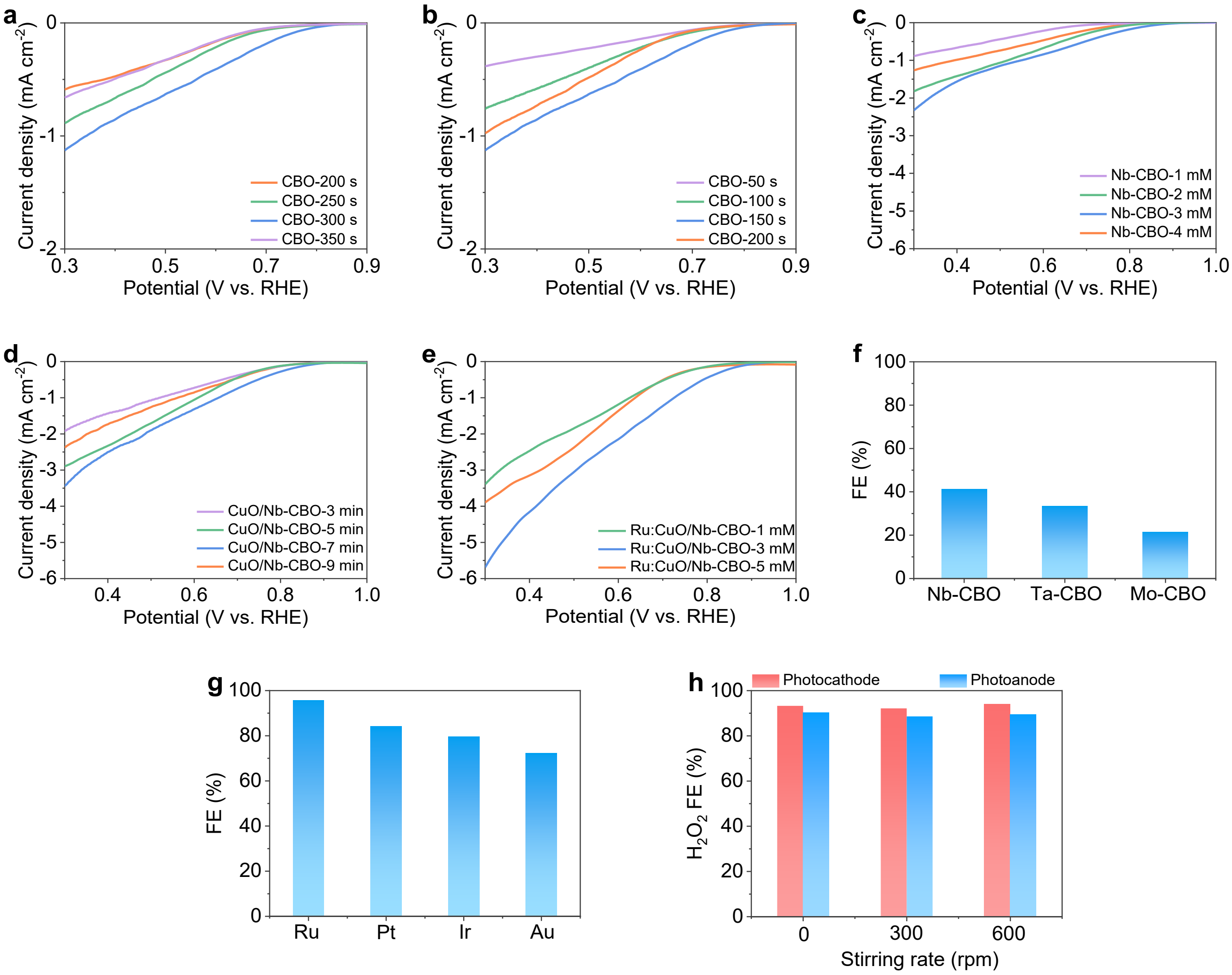

Supplementary Fig. 40 a LSV curves of CBO with various Cu deposition times. **b** LSV curves of CBO with various BiOI deposition times. **c** LSV curves of Nb-CBO with various concentrations of niobamyl oxalate. **d** LSV curves of CuO/Nb-CBO with various Cu sputtering time. **e** LSV curves of Ru:CuO/Nb-CBO with various concentrations of Ru(acac)$_2$. **f** FEs of CBO with different dopant elements. **g** FEs of CuO/Nb-CBO with different catalyst elements. **h** FEs of H_2O_2 for photoanode and photocathode at various stirring rates.

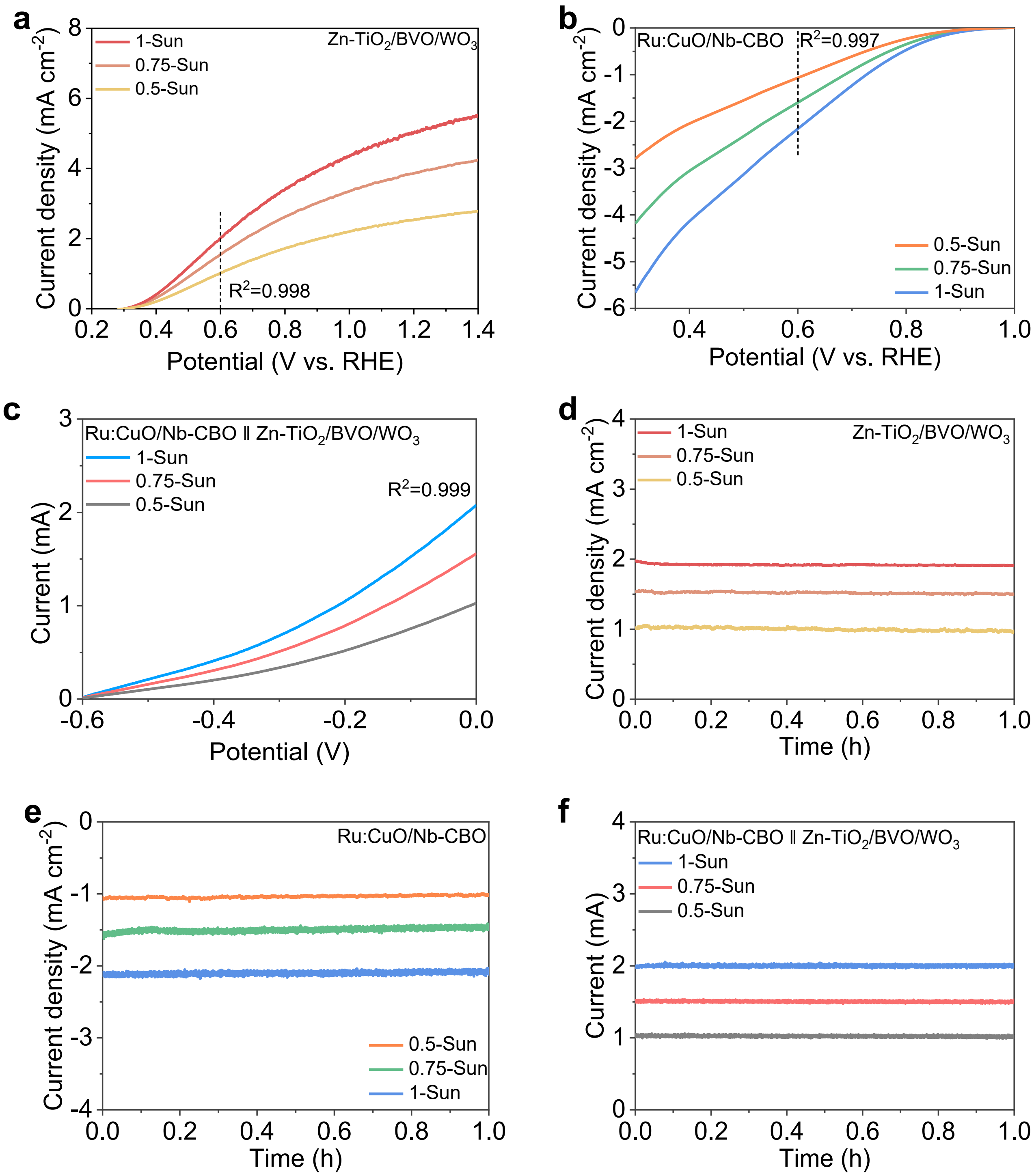

Supplementary Fig. 41 a-c LSV curves of **a** Zn-TiO$_2$/BVO/WO$_3$, **b** Ru:CuO/Nb-CBO, and **c** unbiased tandem system with various light intensities. **d-f** *I-t* curves of **d** Zn-TiO$_2$/BVO/WO$_3$,**e** Ru:CuO/Nb-CBO, and **f** unbiased tandem system with various light intensities.

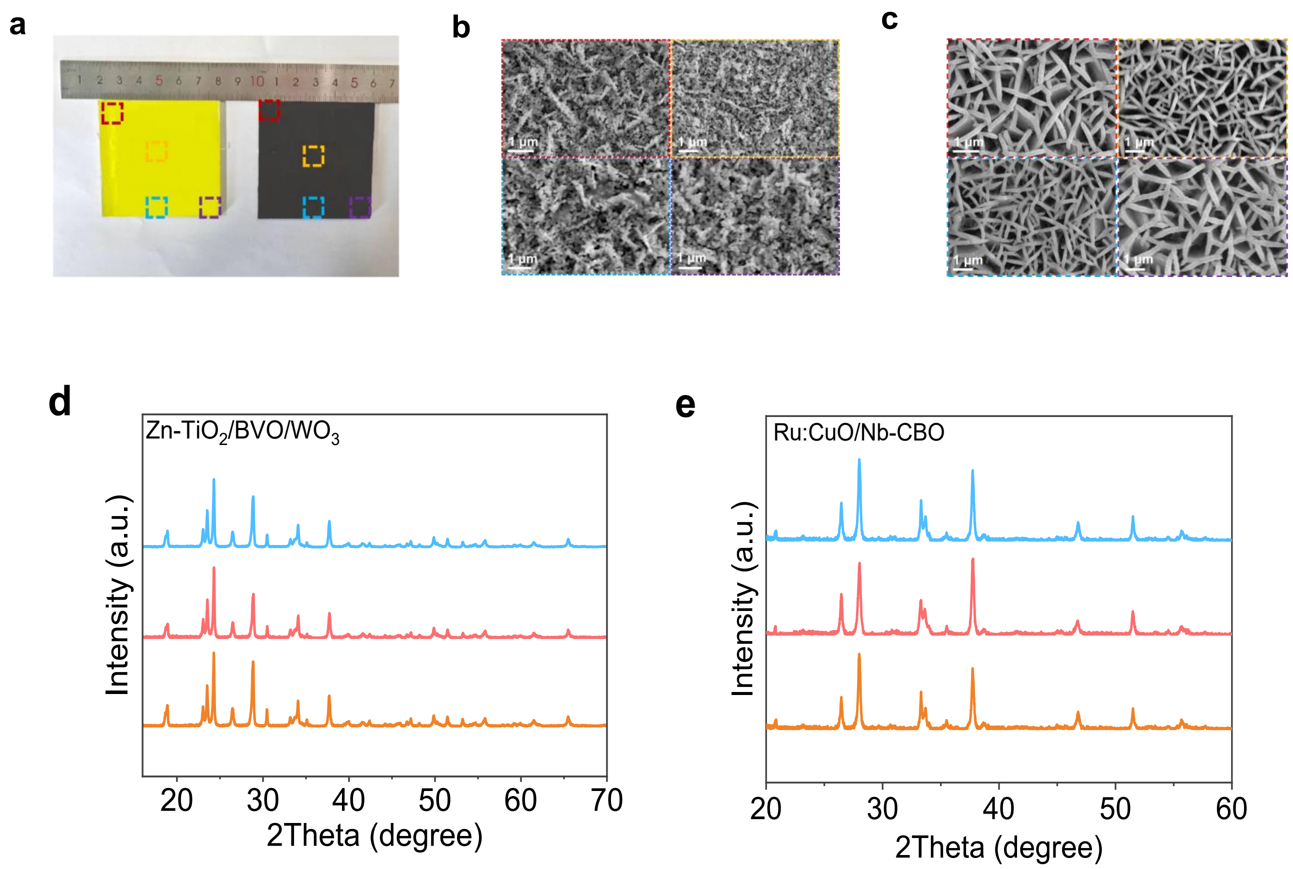

Supplementary Fig. 42 **a** Images of the photoelectrode. **b**, **c** SEM images of all regions to **b** Zn-TiO_2/BVO/WO_3 and **c** Ru:CuO/Nb-CBO. **d**, **e** XRD patterns of all regions to **d** Zn-TiO_2/BVO/WO_3 and **e** Ru:CuO/Nb-CBO.

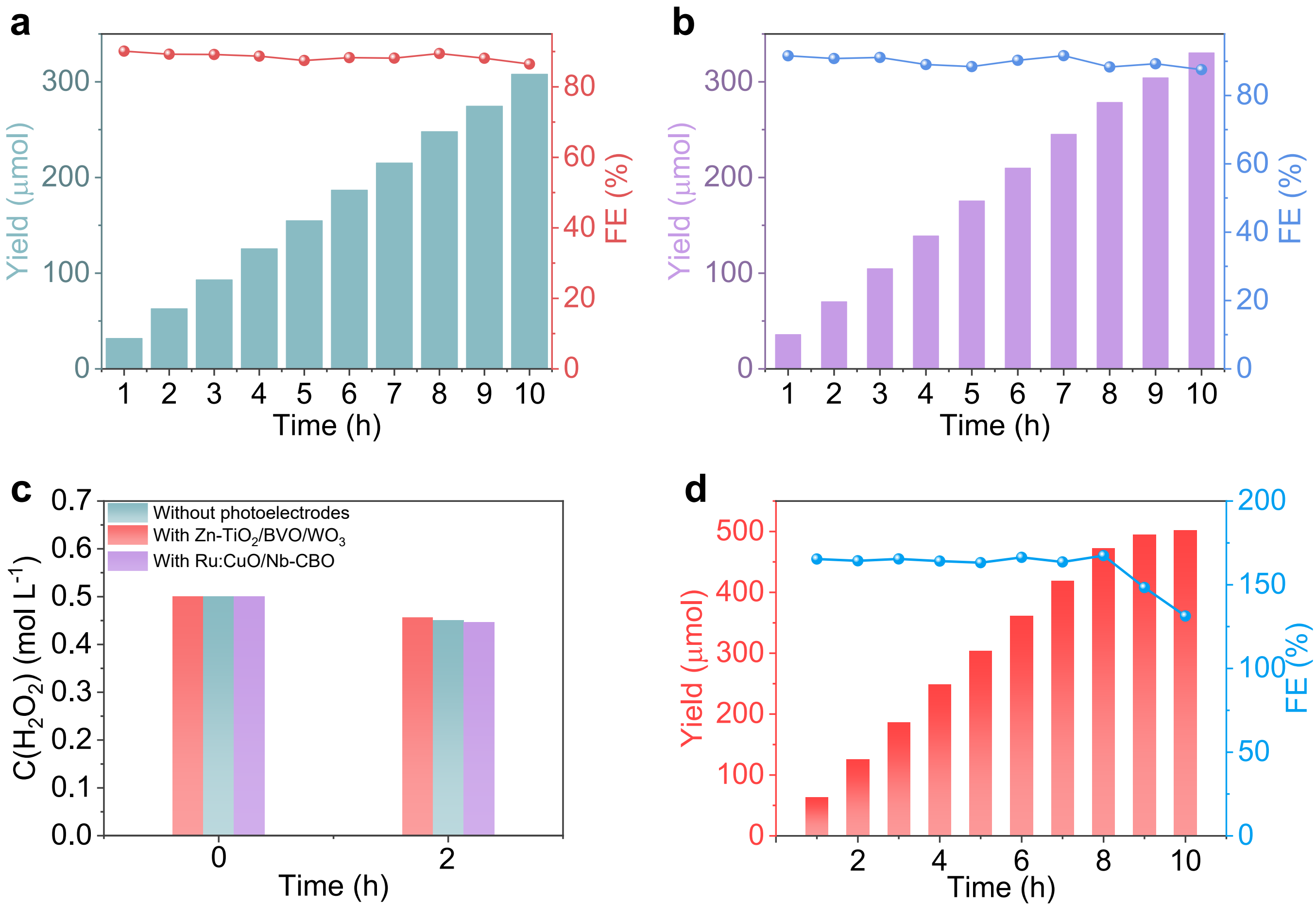

Supplementary Fig. 43 **a** Accumulated H_2O_2 yields and FEs on Zn-TiO_2/BVO/WO_3 during 10 h operation at 0.6 V_{RHE}. **b** Accumulated H_2O_2 yields and FEs on Ru:CuO/Nb-CBO during 10 h operation at 0.6 V_{RHE}. **c** Control decomposition tests with pre-added 0.5 M H_2O_2 (The electrolyte volume was fixed at 30 mL). **d** Accumulated H_2O_2 yields and FEs on unbiased Ru:CuO/Nb-CBO ∥ Zn-TiO_2/BVO/WO_3 in a membrane-free system during 10 h of operation. The surface areas of photoelectrodes were 1 cm^2.

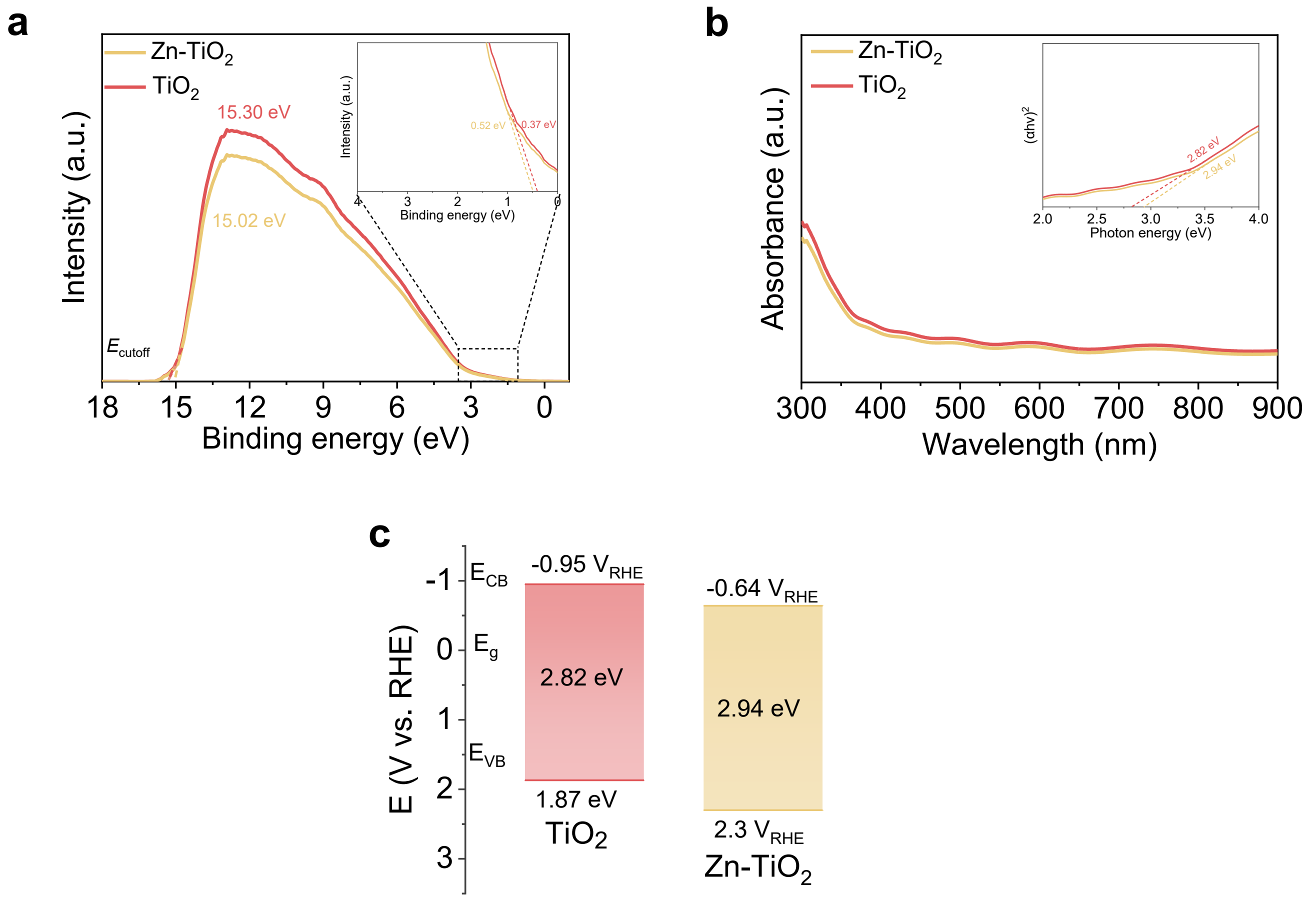

Supplementary Fig. 44 **a** UPS spectra of TiO_2 and Zn-TiO_2. Inset shows the zoomed-in image area in the black dashed lines. **b** UV-vis spectra of TiO_2 and Zn-TiO_2. Inset shows the optical band gaps. **c** Band alignments of TiO_2 and Zn-TiO_2.

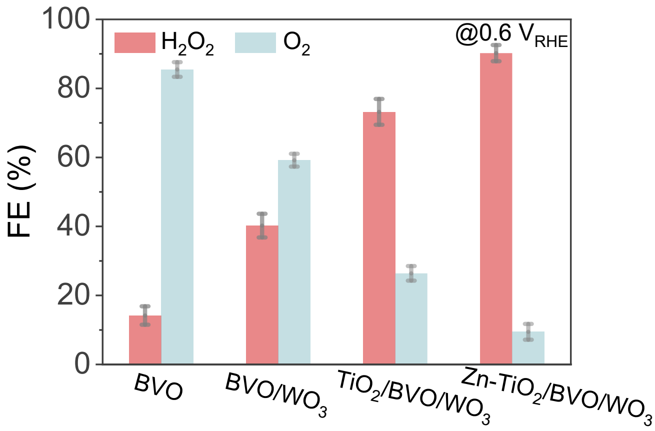

Supplementary Fig. 45 FEs of H_2O_2 and O_2 at 0.6 V_{RHE} for BVO, BVO/WO_3, TiO_2/BVO/WO_3, and Zn-TiO_2/BVO/WO_3.

Supplementary Table 1 Elemental contents of BVO, BVO/WO_3, TiO_2/BVO/WO_3, and Zn-TiO_2/BVO/WO_3 measured by XPS measurements.

Sample	Bi (at.%)	V (at.%)	O (at.%)	W (at.%)	Ti (at.%)	Zn (at.%)
BVO	15.24	15.75	68.99	——	——	——
BVO/WO_3	10.26	10.69	74.23	3.81	——	——
TiO_2/BVO/WO_3	6.80	6.06	73.91	2.74	10.47	——
Zn-TiO_2/BVO/WO_3	5.32	5.48	73.19	2.54	10.28	3.19

Supplementary Table 2 Summary of PEC WOR H_2O_2 performance of recently reported photoanodes under AM 1.5G illumination.

Sample	Electrolyte	η_{H2O2} (μmol cm^{-2} min^{-1})	FE (1.23 V_{RHE})	J(mA cm^{-2}) (1.23 V_{RHE})	Stability	Reference
Zn-TiO_2/BVO/WO_3	1 M $NaHCO_3$ (pH 10)	1.469 (1.23 V_{RHE})	90.2%	5.07	10 h	This work.
CPF-CzPB/Mo:$BiVO_4$	1 M $KHCO_3$ (pH 9)	1.23 (1.23 V_{RHE})	94.08%	4.3	120 h	Adv. Mater. 2025, 37, e08326
SnO_{2-x}/$BiVO_4$	1 M $NaHCO_3$ (pH 8.3)	0.825 (1.23 V_{RHE})	88%	~3.8	1 h	J. Am. Chem. Soc. 2020, 142, 8641.
P-Mo-$BiVO_4$	1 M $NaHCO_3$ (pH 8.3)	0.21 (1.0 V_{RHE})	46%	~1.8	5 h	Energy Environ. Sci. 2020, 13, 1730.
$BiVO_4$/Au-PAT	1 M $NaHCO_3$ (pH 8.3)	0.312 (1.23 V_{RHE})	72.10%	~1.66	2 h	ACS Energy Lett. 2023, 8, 5192.
$CaSnO_3$/$SrTiO_3$/$BiVO_4$	1 M $NaHCO_3$ (pH 8.3)	0.825 (1.2 V_{RHE})	90%	~2.99	3 h	ACS Energy Lett. 2024, 9, 1415.
N-O_{vac}-$BiVO_4$-350	1 M $NaHCO_3$ (pH 8.3)	~0.76 (1.6 V_{RHE})	81.20%	~2.9	2 h	ACS Energy Lett. 2022, 7, 3024.
O-$BiVO_4$	2 M $KHCO_3$	---	42.80%	~0.5	---	ACS Catal. 2024, 14, 5297.
Ni_5P_4/NiO/$BiVO_4$	2 M $KHCO_3$	0.313 (1.2 V_{RHE})	76.5%	4.05 (1.78 V_{RHE})	---	Chem. Eng. J. 2025, 510, 161667.
ZnO/$BiVO_4$	2 M $KHCO_3$	---	31.60%	2.83	10 min	J. Energy Chem. 2025, 103, 877.
Co_3O_4@Pt-Fe_2O_3	2 M $KHCO_3$	0.073	77.38%	1.35	---	Chem. Eng. J. 2023, 473, 145384.
$ZnIn_2S_4$-Se/QDs	1 M $NaHCO_3$ (pH 8.3)	---	86%	4.2	7 h	Chem. Eng. J. 2024, 491, 151925.
A-TP/TiO_2	1 M $KHCO_3$ (pH 9)	0.225 (1.76 V_{RHE})	63%	0.46 (1.76 V_{RHE})	---	J. Energy Chem. 2023, 86, 399.

Supplementary Table 3 Fitting results of the EIS measurements for BVO, BVO/WO_3, TiO_2/BVO/WO_3, and Zn-TiO_2/BVO/WO_3.

Sample	R_s (Ω)	R_{trap} (Ω)	C_{bulk} (×10^{-6} F)	R_{ct} (Ω)	C_{ss} (×10^{-5} F)
BVO	48.27	423.8	4.82	348.5	1.357
BVO/WO_3	46.59	215.2	4.16	263.7	1.368
TiO_2/BVO/WO_3	41.25	248.1	3.97	232.4	1.649
Zn-TiO_2/BVO/WO_3	38.13	146.3	5.20	227.9	1.682

Supplementary Table 4 ICP analysis of electrolytes for Zn-TiO_2/BVO/WO_3 after 10 h i-t measurements and Ru:CuO/Nb-CBO after 50 h i-t measurements.

Sample	Zn (mg/L)	Ti (mg/L)	V (mg/L)	W (mg/L)	Bi (mg/L)	Cu (mg/L)	Ru (mg/L)	Nb (mg/L)
Zn-TiO_2/BVO/WO_3	0.17	0.38	0.03	0.01	0.03	---	---	---
Ru:CuO/Nb-CBO	---	---	---	---	0.02	0.34	0.18	0.03

Supplementary Table 5 Summary of PEC ORR H_2O_2 performance of recently reported photocathodes under AM 1.5G illumination.

Sample	Electrolyte	Stability	FE (0.6 V_{RHE})	Onset potential (V_{RHE})	Reference
Ru:CuO/W-CBO	**1 M $NaHCO_3$ (pH 10)**	**50 h**	**91.93%**	**1.0**	**This Work.**
CPF-CzAD	1 M $KHCO_3$ (pH 9)	120 h	90.8 %	---	Adv. Mater. 2025, 37, e08326
O-BP/FM-PSK	0.1 M KOH	12 h	100%	0.85	Nat. Commun. 2021, **12**, 6644.
Cu_3BiS_3/CdS/TiO_2/MoO_x/Mo	0.2 M KOH	14 h	100%	0.9	Energy Environ. Sci. 2024, **17**, 5588.
Au/$CuBi_2O_4$/$PtSe_2$	0.1 M $KHCO_3$	3 h	35%	1.0	Adv. Funct. Mater. 2023, **33**, 2303391.
$Na_2Co_2O_4$/$CuBi_2O_4$	0.1 M $KHCO_3$ with 0.1 M $Na_2S_2O_8$	1 h	47.42%	1.0	App. Catal. B 2022, **304**, 120980.
Au-In_2S_3/Cu_3BiS_3	0.1 M PBS	2 h	71%	0.5	Appl. Catal. B 2022, **307**, 121152.
O-BP/FM-PSK	0.1 M KOH	12 h	100%	0.85	Nat. Commun. 2021, **12**, 6644.

Supplementary Table 6 Fitting results of the EIS for CBO, Nb-CBO, CuO/Nb-CBO, and Ru:CuO/Nb-CBO.

Sample	R_s (Ω)	R_1 (Ω)	CPE_1 (×10^{-6} F)	R_2 (Ω)	CPE_2 (×10^{-5} F)
CBO	35.45	183.2	3.84	199.6	1.34
Nb-CBO	31.24	146.8	3.21	176.8	1.67
CuO/Nb-CBO	36.78	134.6	3.67	186.7	1.95
Ru:CuO/Nb-CBO	33.61	167.4	3.45	169.2	1.88

Supplementary Table 7 Summary of bipolar H_2O_2 performance of recently reported.

System	Sample	Applied bias (V_{RHE})	$\eta_{H_2O_2}$ (µmol cm^{-2} min^{-1})	FE	Stability	Current density (mA cm^{-2})	Reference
PEC ‖ PEC	**Zn-TiO_2/BVO/WO_3‖ Ru:CuO/Nb-CBO ‖**	**unbiased**	**1.07**	**Total:163.37%**	**10 h**	**2.08**	**This work.**
PEC ‖ PEC	CPF-CzPB/Mo:$BiVO_4$ ‖ CPF-CzAD	unbiased	1.083	---	~168 h	1.85	Adv. Mater. 2025, 37, e08326
PEC ‖ PEC	$CaSnO_3$/SnO_2/$BiVO_4$ ‖ PV	unbiased	---	Photoanode:90%	5 h	5.77	Adv. Energy Mater. 2026, 16, e05447.
PEC ‖ EC	RuOx/TNR‖ AQ-graphite	unbiased	---	Total:90%	100 h	1.23	Energy Environ. Sci. 2021, 14, 3110.
PEC ‖ EC	P-Mo-BVO‖ AQ-CNT/C	unbiased	0.16	Photoanode:43% Cathode:100%	5 h	---	Energy Environ. Sci. 2020, 13, 1730.
EC ‖ EC	O-CNTs ‖ PTFE-C	1.7	24	Total:153%	~3 h	120	Nat. Catal. 2020, 3, 125.
EC ‖ EC	D-PSFZ ‖ D-PSFZ	2.1	---	Total:163%	100 h	50	Nat. Commun. 2023, 14, 5822.

Supplementary Table 8 Areal production rates and SCC efficiencies.[3-5]

Electrode area (each)	Current (mA)	Combined FE (%)	$Yield_{H_2O_2}$ (mM)	Areal production rate (μmol cm^{-2} h^{-1})	SCC (%)
20 cm^2	24.78	165.38	7.64	19.1	0.86
36 cm^2	37.54	163.37	11.44	15.9	0.72

Supplementary Discussion: Outdoor tests were performed under natural sunlight with an average intensity of 72 mW cm^{-2} (0.72 sun). The electrolyte volume was 100 mL in a single-compartment (PEM-free) cell. Two sets of photoelectrodes (Zn-TiO_2/BVO/WO_3 anode + Ru:CuO/Nb-CBO cathode) with different areas were tested for 1 h. The results are summarized in the table.

The areal H_2O_2 production rate (R_A, in μmol cm^{-2} h^{-1}) is defined as:

$$R_A = \frac{C \times V}{A \times t}$$

where C is the measured H_2O_2 concentration (μmol L^{-1}), V is the electrolyte volume (L), A is the total geometric area of the photoelectrode (cm^2; for the unbiased cell, both electrodes have the same area), and t is the illumination time (h).

The solar-to-chemical conversion (SCC) efficiency for H_2O_2 production is defined as:

$$SCC = \frac{\Delta G \times (n_{H2O2,anode} + n_{H2O2,cathode})}{P_{solar} \times A_{cell} \times t} \times 100\%$$

where ΔG = 117 kJ mol^{-1} is the standard Gibbs free energy of H_2O_2 formation from H_2O and O_2 (averaged for the two half-reactions), n is the total amount of H_2O_2 (mol) produced at both electrodes, P_{solar} is the solar power density (100 mW cm^{-2} for AM 1.5G; measured value for outdoor test), and A_{cell} is the illuminated area (same as electrode area, since both electrodes are illuminated in our tandem configuration). For outdoor tests, we used the measured average sunlight intensity (≈72 mW cm^{-2} on the test day).

The areal production rate is calculated based on the total illuminated area (anode + cathode, both illuminated in the tandem configuration). For the 20 cm^2 electrodes, total illuminated area = 40 cm^2, giving a rate of 19.1 μmol cm^{-2} h^{-1}; for the 36 cm^2 electrodes, total illuminated area = 72 cm^2, giving a rate of 15.9 μmol cm^{-2} h^{-1}. (If expressed per single electrode area, the values would be twice as high: 38.2 and 31.8 μmol cm^{-2} h^{-1}, respectively.) The SCC efficiency was calculated using the Gibbs free energy of H_2O_2 formation (117 kJ mol^{-1}) and the measured total H_2O_2 amount. Under 0.72 sun natural sunlight, the SCC values are 0.86% for the 20 cm^2 electrodes and 0.72% for the 36 cm^2 electrodes.

Supplementary References

1. Moon, S., Park, Y. S., Lee, H., Jeong, W., Kwon, E., Lee, J., Yun, J., Lee, S., Kim, J. H., Yu, S., Moon, J. *Energy Environ. Sci.* **17**, 5588 (2024).
2. Mehrotra, R., Oh, D., Jang, J.-W. *Nat. Commun.* **12**, 6644 (2021).
3. Wang, L., Guo, F., Ren, S., Gao, R.-T., Wu, L. *Angew. Chem. Int. Ed.* **63**, e202411305 (2024).
4. Wang, L., Wu, Y., Mao, S., Zhou, J., Zhang, Y., Zheng, X., Wu, X., Xu, H. *Adv. Mater.* **37**, e08326 (2025).
5. Ye, Y. -X., Pan, J., Shen, Y., Shen, M., Yan, H., He, J., Yang, X., Zhu, F., Xu, J., He, J., Ouyang, G. *Proc. Natl. Acad. Sci. U.S.A.* **118**, e2115666118 (2021).